NUMERICAL AND EXPERIMENTAL INVESTIGATIONS ON THE ZETA POTENTIAL OF DIFFERENT SIZE MESOPOROUS SILICA NANOPARTICLES WITH DIFFERENT POROUS PROPERTIES

A Thesis Submitted to
the Graduate School of Engineering and Science of
İzmir Institute of Technology
in Partial Fulfillment of the Requirements for the Degree of

MASTER OF SCIENCE

in Biotechnology

by
Fetiye Esin YAKIN

July 2020
İZMİR

ACKNOWLEDGMENTS

I would like to tell my sincere gratitude to my advisor Assoc. Prof. Dr. Murat BARIŞIK for his continuous support and motivation during my studies, research, and master. I am sincerely thankful to him for his guidance and for sharing his experience and knowledge with me during my master studies.

As a part of Micro/nano Engineering (MiNaEng) Research Group, I would like to acknowledge several of my colleagues for their support and contributions. I would like to thank Tümcan ŞEN for his help and for sharing his experience with me from the beginning of my studies. Also, I am thankful to Büşra Öykü ALAN as my project partner, for her support and contributions during this project. Moreover, I would like to send my love to Fikrican Dilek for his support whenever I need him during my master's study. I would like to acknowledge my sincere gratitude to all of my colleagues from the research group.

We would like to thank The Scientific and Technological Research Council of Turkey (TUBITAK), for allowing us to carry out this research. This work is supported by TUBITAK under the grant number 118M710. This work was also supported by the BAGEP Award of the Science Academy.

I would like to send my most sincere gratefulness to my mother for her limitless support, encouragement, and love during my studies and whole life.

ABSTRACT

NUMERICAL AND EXPERIMENTAL INVESTIGATIONS ON THE ZETA POTENTIAL OF DIFFERENT SIZE MESOPOROUS SILICA NANOPARTICLES WITH DIFFERENT POROUS PROPERTIES

Mesoporous silica nanoparticles (MSN) are utilized by many applications due to their high surface to volume ratio, tunable pore size, low toxicology, and colloidal stability. These properties make silica nanoparticles good candidates for targeted drug delivery applications. Targeted drug delivery steps include cellular internalization, endosomal escape, and cargo release to the selective tissue. The geometric properties of MSN such as particle size, pore size, and porosity, as well as surface chemistry and resulting surface charge density determine the MSN behavior in these steps. This study examines the influence of particle size, pore size, and porosity of an MSN to its surface zeta potential. We performed both numerical and experimental investigations. The zeta potential of various MSNs at different salt concentrations was calculated by solving the Poisson-Nernst-Planck equation with active surface charge boundary conditions considering surface chemistry. We validated our multi-ion model through experiments. Results indicate that zeta potential exhibits a strong dependence on particle size, pore size, and porosity. By increasing porosity and/or pore size, the absolute average zeta potential decreased up to 25% from the theoretical predictions. Second, zeta potentials of silica particles at different sizes and surface areas were experimentally measured at different salt concentrations. Particles were systematically characterized by measuring particle size using Dynamic Light Scattering (DLS), analyzing chemical properties using Fourier-transform infrared spectroscopy (FTIR), measuring surface area using Brunauer–Emmett–Teller (BET) analysis, and imaging using Scanning Electron Microscopy (SEM). A well-dispersed solution in colloidal stability was obtained by systematically tuning corresponding parameters. The absolute average zeta potential was found to increase with a decrease in particle size, while zeta potential was found to decrease with a decrease in surface area at a constant particle diameter, similar to numerical calculations.

Keywords: Mesoporous Silica Nanoparticles; Surface Zeta Potential, Porosity, Pore Size, Colloidal Stability.

ÖZET

FARKLI GÖZENEK ÖZELLİKLERİNE SAHİP FARKLI BOYUTLARDAKİ MEZOPORLU SİLİKA NANOPARÇACIKLARIN ZETA POTANSİYELİNİN DENEYSEL VE NÜMERİK İNCELENMESİ

Mezopor silika nanoparçacıkları (MSN) yüksek yüzey / hacim oranı, ayarlanabilir gözenek boyutu, düşük toksikoloji ve koloidal stabilitesi nedeniyle birçok uygulama tarafından kullanılmaktadır. Bu özellikler, silika nanopartiküllerini, hedeflenen ilaç verme uygulamaları için iyi adaylar kılar. Hedeflenen ilaç verme aşamaları arasında hücresel içselleştirme, endozomal kaçış ve seçici dokuya kargo salımı yer alır. MSN'in parçacık boyutu, gözenek boyutu ve gözeneklilik gibi geometrik özellikleri, yüzey kimyası ve sonuçta oluşan yüzey yük yoğunluğu bu adımlarda MSN davranışını belirler. Bu çalışma, bir MSN'nin parçacık büyüklüğü, gözenek boyutu ve gözenekliliğinin yüzey zeta potansiyeline etkisini incelemektedir. Hem sayısal hem de deneysel araştırmalar yapıldı. Farklı tuz konsantrasyonlarında çeşitli MSN'lerin zeta potansiyeli, yüzey kimyası göz önünde bulundurularak, Poisson-Nernst-Planck denkleminin aktif yüzey yükü sınır koşulları ile çözülmesiyle hesaplanmıştır. Çok iyonlu modelimizi deneylerle doğruladık. Sonuçlar, zeta potansiyelinin parçacık boyutu, gözenek boyutu ve gözenekliliğe güçlü bir bağımlılık gösterdiğini göstermektedir. Gözenekliliği ve/veya gözenek boyutunu artırarak, mutlak ortalama zeta potansiyelini teorik tahminlerden% 25'e kadar azalmıştır. İkinci olarak, farklı boyutlarda ve yüzey alanlarındaki silika parçacıklarının zeta potansiyelleri, farklı tuz konsantrasyonlarında deneysel olarak ölçülmüştür. Parçacıklar sistematik olarak Dinamik Işık Saçılımı (DLS) kullanılarak parçacık boyutunun ölçülmesi, Fourier Dönüşümü Kızılötesi Spektroskopisi (FTIR) kullanılarak kimyasal özelliklerin analiz edilmesi, Brunauer – Emmett – Teller (BET) analizi kullanılarak yüzey alanının ölçülmesi ve Taramalı Elektron Mikroskobu (SEM) ile görüntü alınması gibi deneysel adımlara tabi tutulmuştur. Kolloidal stabilitede iyi dağılmış bir çözelti, karşılık gelen parametrelerin sistematik olarak ayarlanmasıyla elde edildi. Mutlak ortalama zeta potansiyelinin parçacık boyutunda bir azalma ile arttığı, zeta potansiyelinin ise sayısal hesaplamalara benzer şekilde sabit bir parçacık çapındaki yüzey alanında bir azalma ile azaldığı bulunmuştur.

Anahtar Kelimeler: Mesopor Silika Nanoparçacıklar, Yüzey Zeta Potansiyeli, Gözeneklilik, Gözenek Boyutu, Kolloidal Stabilite.

TABLE OF CONTENTS

LIST OF FIGURES

Figure **Page**

Figure **Page**

LIST OF TABLE

LIST OF SYMBOLS

C_{i0}	The bulk concentration of i^{th} ion	
C_{KCl}	The bulk concentration of KCl	mM
D_i	Diffusivity of i^{th} ion	m^2 / s
E	Electric field	N / C
F	Faraday constant	C / mol
K_A, K_B	Equilibrium constants	
N_{total}	Total number of the site functional groups	$sites / nm^2$
pH	pH level	
Dpore	The diameter of the 3-D pore size	nm
$D_{Particle}$	Diameter of particle	nm
H	Pore Size	nm

Greek Letters

ε_0	The relative permittivity of vacuum	F / m
ε_r	The relative permittivity of ionic liquid	F / m
σ_s	Surface charge density	C / m^2
λ	Debye length	nm
ψ	Electric potential distribution	V / m
Γ	Surface site density	$sites / nm^2$
Є	Porosity	X
Θ	Theta	°
ζ	Zeta Potential	mV
η	Dynamic viscocity	cP
μ_e	Electron mobility	$cm^2/(V.s)$
n	Refractive index	X
λ	EDL Thickness	nm

Subscripts

DLS	Direct Light Scattering
MSN	Mesoporous Silica Nanoparticle
SEM	Scanning Electron Microscope
APA	Ammonium Salt of Polyacrylate

CHAPTER 1

INTRODUCTION

In recent years, the mesoporous silica nanoparticles (MSNs) have been applied as trend research in both natural science and engineering areas. The content of silica is about 75% in the earth's rocks and plants[1]. Therefore, the silica has been started to use in every scientific area because of its significant source. Health humans contain an average of 260 ppm silica in their bodies[2, 3]. Therefore, the utilization of various silica nanoparticles has been started in the bioengineering area as a biomaterial by scientists[4]. The large surface to volume ratio, high loading capacity, thermal stability strength, and low toxicology chemical environment are unique properties of MSNs. These all properties of silica nanoparticles make them good biodegradable material for biomedical science areas such as bio-imaging for diagnostics[5], bio sensing[6], bio catalysis[7], drug delivery[8], gene delivery[9], gene therapy[10], and anticancer therapeutic agents[11]. Hence, the unique tunable properties of MSNs need to discover in the mesoporous colloidal system because of finding their effect on the bio-applications[12]. However, the application of MSNs has an unexplored area due to their physical and chemical possessions that cannot be explained by literature in biomedical science, yet.

The first mesoporous silica nanoparticle was synthesized as a monodisperse particle by Ströber et al. in the 1970s. The experimental procedure of synthesis to monodisperse silica nanoparticle was obtained to react of tetra alkyl silicate with hydrolysis into the alcohol and water liquid media at room temperature[13]. In the ’90s, the first mesoporous silica nanoparticle was synthesized successfully by the improvement of the reaction procedure by added to the catalyst into the reaction medium[14]. The MSNs are sorted as mesoporous due to their pores’ size between 2-50 nm, and the diameter of nanoparticles is less than 500nm[15]. The various MSN type is synthesized by alteration of pH, temperature, and catalyst. The sol-gel and spray drying synthesis procedures are the most used methods of acquiring MSNs for requested synthesis[16]. The sol-gel synthesis procedure mainly comprises a colloidal particle in a sol. Also, the solution contains the organosilane-precursor and water liquid into the media. The synthesis process is divided into two parts: hydrolysis and condensation. The chemical

reaction leads to highly porous gel silica sample solutions produced as a powder, 3D, 2D, and 1D materials.[17]. The main advantages of the sol-gel chemical process are that it is time-saving, cost-effective, and governable. The spray drying method obtains that the silica precursor and volatile solution react with each other. The surfactant additives allow us to obtain spherical mesoporous as a final product into the drying chamber. The reaction coincides concerning initial stoichiometry ratios. The cargo loading capacity of MSNs is decided by the spray drying method, which permits to carry more than one active site of drug molecules [18]. The most well-known MSNs are named according to their geometrical structures, which belong to families that MCM (Mobile Composition of Matter) and SBA (Santa Barbara Amorphous) type MSNs, for instance, MCM-41, MCM-48, SBA-15, and SBA-16. The first synthesized MSN was MCM-41 that has a 2D hexagonal structure[19]. After altering thermal hydrodynamic situations and utilizing catalysts as a precursor, the SBA type of silica mesoporous particles has been appeared in the scientific literature[20-22]. Figure 1.1 demonstrates that SEM images of SBA-15 mesoporous nanoparticle were obtained highly curved shape after production, spontaneously [23, 24]. Their structures of MSNs such as the rod spheres, cylinder, and cube shapes have been tended to use in targeted drug delivery mechanisms according to their tunable accumulation features[25-28].

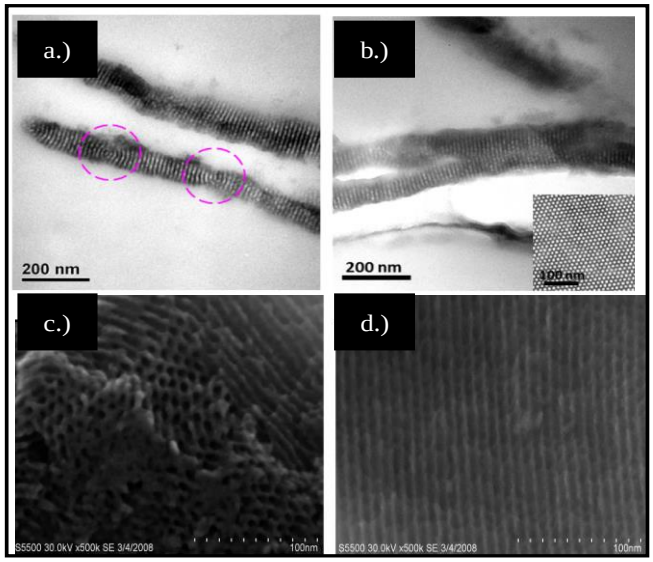

Figure 1.1. 2D SBA-15 Mesoporous Silica Nanoparticles ((a&b), D_p=100 nm) developed in Yeh et al. (Source: 23) - Published by The APL Materials. Hexagonal SBA-15 of Mesoporous Silica Nanoparticles((c&d), D_p=100nm) synthesized in Tuysuz et al. (Source:24) - Published by Journal Of American Chemical Society.

The MSN efficiency at the targeted drug mechanism is directly proportionate with high loading capacity of drug and time -dependence cargo release percentage at cardiovascular tumor cells where reach the target tissue. Furthermore, MSNs improve the drug carrier mechanism's efficiency and reduce the side effect of biochemical reactions[29]. The nanoparticles penetrate to the vascular barriers of carcinoma blood vessels from the mother vessels' side; then, these vessels contain rich protein plasmas and blood cells, which result in high blood pressure[30]. The extracellular matrix and media provide nanoparticles moving to tumor area during exact less time and interact with the cellular membrane's phospholipids. Moreover, the MSNs are decreased to cytotoxicity by coordinate with the oxidative stress level of reactive oxygen side and repress the glutathione levels that lead to the death of cancer tumors[31]. MSN's main drawback is to be described as an endosomal escape mechanism during the utilization of targeted drug delivery. Firstly, the nanoparticle appears as a remarkable compound when it circulates in the cell. The protection mechanism of the endosome sends its enzymes for the digestion of nanoparticles. Hence, the ionic concentration and surface charge environment of nanoparticle give primary information about behaviors of endosomal escape reaction. The most common method for being successful in the endosomal escape mechanism is named as a proton sponge effect[32]. The increases of ionic concentration support escaping to nanoparticle from endosome to cytosol. Because, the sharply increased concentration of Cl^- ions assist MSN to exit from endosome to cytosol till the channel of Cl^- because of osmatic swelling. The experimental studies point out that the MSN, which covers with negative surface charge, is easy to be completed endosomal escape mechanism, and the yield of releasing cargo increases according to cationic surface charged nanoparticles [33]. Moreover, the scientist developed other strategies for controlling the circulation of nanoparticle during the cellular uptake. A passive targeting mechanism is another strategy that controlling migrations of nanoparticle with specific physical parameters, which are particle size, morphology, and the surface hydrophobicity of nanoparticle[34]. The studies show that the optimum particle diameters of MSN should be between 100 to 200 nm. Moreover, the faster acceleration of MSNs is observed in liver and lung tissues because of the high blood flow rate[35]. Therefore, the enhanced permeability and retention effect (EPR) is employed that controls the acceleration behavior for solid tumor cells. According to an EPR effect, the MSN tends to accumulate the carcinoma cells more than healthy cells through the blood vessels. The endothelial cells of tumors have disordered cell shape, gaps, and tubular flow so, EPR effects contribute to the movement

of nanoparticles through the gaps in terms of their morphologies[36]. Because the results of passive targeting mechanism linearly proportional with physical parameters of MSN, therefore, the surface charged characterization displays to the critical role of why MSN should be developed during the targeted drug delivery mechanism.[37, 38]

The effects of surface charge on the nanoparticle allow giving a variety of information about the characterization of MSNs. The hydrophobicity and surface charge are significant parameters to expect the behavior of the cellular uptake process. The surface charge decides the behaviors of nanoparticle interaction with the receptors of the cell membrane. Because the cell membrane contains phospholipids and phosphatidylserine compounds so, these compounds make the cell membrane as a negative charge[39]. The cell membrane tends to uptake positively charged molecules inside effortlessly. Furthermore, the various geometric features affect the interaction between the cell membrane and nanoparticle uptake. Generally, the uptake reaction obtains in a higher yield percentage where the diameter of MSN is larger than 100 nm[10]. However, the surface charge and magnitude of zeta potential value give a clue about the circulation movement of MSN where the tumor part of the tissue. The experimental results point out that the zeta potential (ζ) magnitude range, where between -10mV to +10mV, produces a long time motion of MSN into the cancer cell[40]. Mei et. al. showed that the medium salt concentration and neutral pH value had extended mobility time effect of small diameters MSNs into the blood vessels[41]. Nevertheless, there are no studies about the effect of high ionic media interact with a larger diameter of MSNs whose diameter is more than 200 nm. The ionic intermolecular interaction of the MSN surface between silanol groups with the cell membrane's recognition compounds constitutes the electric double layer (EDL) on the surface of MSNs so, the value of zeta potential is directly proportional with the EDL thickness. Besides, the protonation and deprotonation reactions with silanol groups and counter ions are major determinations of the overall surface charged on nanoparticles[42-44]. The surface charge depends on either the pH value of the chemical environment or the concentration of counterions. As a result of chemical equilibrium on the surface, the tendency behavior of ionic distribution is explained with Boltzmann distribution theory. The theory is solved by applying the Poisson-Boltzmann (PB) equation[45]. However, this PB equation only validates certain conditions that are flat particle; the magnitude of zeta potential should be smaller than -25 mV. On the other hand, the mesoporous environment cannot be explained with the PB

equation. Because several physical conditions lead to inaccurate measurement of surface charge on MSN. Firstly, the thickness of the EDL proportionally relates to the bulk concentration. The less ionic environment causes higher EDL overlap on the surface of the mesoporous nanoparticle[46-48]. Secondly, the curvature effect occurs where the nanoparticle diameter decreases because of the decrease of a surface to volume ratio of MSN. Furthermore, the physical differences of the entrance on pore throat are another reason for improving the curvature effect on the surface of the mesoporous nanoparticle [49, 50]. All the above leads to an estimate of chemical equilibrium incorrectly on the pore surface of nanoparticles. This chemical equilibrium is the critical understanding of mechanism surface charge reactions between silica and loading cargo so, The Poisson-Nernst –Planck Equation assists to explain the ionic condition on the surface of nanoparticle without Boltzmann distribution simplification. The PNP equation is not enough to shows the electrical charging on the surface because of the media's hydronium ion reactivity. Because the EDL overlap impacts the surface charge on the surface where consists of constant potential boundary and surface charge condition. However, the EDL overlap on the surface creates their local variations that the new equilibrium environment demonstrates their surface charge variation where it does not remain constant at the local surface area. Therefore, the charge regulation model was developed to explain nature chemistry on the nanoparticle surface.[51, 52] The first breakthrough of the charge regulation model was applied to the colloidal science and AFM measurements by Ninham and Parsegian [53]. After CR modeling includes the analytical calculations, the boundary conditions are easily calculated correctly with this method, and the trend of utilization of CR modeling increases in numerical calculation methods. The development of the multi-ion charge regulation method points out understanding the electrokinetic variations on the surface of MSNs where the characterizations of them are appropriately executed.

According to previous studies, the multi-ion active charge regulation model was developed to measure the nanoparticles' local surface charge, where alters of their geometrical and physical features, for solved assorted values of electric potential responses[54]. Previous works demonstrated that various ionic concentrations of the environment instantly impacted the calculation of surface charge on nanoparticle so, the characterization of MSN depended on the local chemical equilibrium environment between the pore inside and the surface of MSN. Moreover, the effect of EDL overlap resulted from a pore size ratio, the diameter of nanoparticle, porosity, and local ionic condition on the surface of MSN. Furthermore, the higher porosity and less ionic

conditions interaction values help develop MSN's curvature effect. In our study, the effect of small and large diameter on MSNs was worked to display the variation on ζ-potential values with the dependence of the ionic condition environment. The EDL overlap and curvature effect were observed on the surface of the small-diameter nanoparticles (50 nm) in the lack of repulsive force between intermolecular interaction. However, the dominant effect of a repulsive force was developed in the larger diameter of MSNs (330 nm), was eliminated the EDL overlap and curvature effect on the surface of MSNs. Moreover, the pore size and porosity vary systematically, where the variation of ζ-potential values indicated close agreement with theoretical estimations. Besides, experimental studies show similar results with numerical calculations developed by multi-ion active charge regulation model with various pore size, porosity, and size range[55].

This thesis aims to characterize the diameter dependency of the mesoporous silica nanoparticles' zeta potential through numerical analyses, where the ionic concentration, pore size, and porosity are varied. The multi-ion charge regulation of the Poisson-Nernst-Planck equations is solved with different physical parameters. The intermolecular forces between the chemical molecules will be dominated with measured this active charge model on the MSN. A phenomenological model is developed to evaluate the zeta potential of MSNs as a function of the pore volume/diameter ratio. Also, the experimental investigations will be figured out by illustration of colloidal stability and dispersion according to various salt concentrations, the volume of polymeric dispersants, the amount of amorphous silica powder, and pH.

The outline of this work can be explained by followed alignments; in Chapter 2, the literature scientific state of MSNs in targeted drug delivery mechanisms and the theoretical, numerical background will be explained. In chapter 3, the modeling of the experimental procedure will be demonstrated with the main important parameter. In chapter 4, the numerical background will be defined that all contents about numerical analyses demonstrated by figures and equations. Moreover, in chapter 5, all the numerical and experimental results will explain with figures and tables. Finally, in chapter 6, the discussion and conclusion part will be clarified according to numerical and experimental results.

CHAPTER 2

LITERATURE REVIEW

The synthesis of ordered MSNs was discovered by Mobil researchers about 20 years ago [56]. MSNs are the new class of nanoparticles that maintain the pore size between 2-30 nm. The facilities of MSNs, which are porous, highly ordered size, and evaporation-induced self- assembly, have made them utilize as a nanocarrier material in drug delivery applications. MSNs are synthesized with different pore geometries and particle sizes by using different experimental synthesis procedures. The predominant techniques are sol-gel and spray drying methods that synthesize different various types of MSNs with different linkage geometries. The MCM (Mobile Crystalline Materials)-41 was the first synthesis mesoporous silica nanoparticle by the Ströber method. Generally, the structure types of MCM-41 are the 2D hexagonal and 3D hexagonal with uni-directional pore structure. The pore size ranges of MCM-41 are 1.5-4 nm [57, 58]. Another MCM type is the MCM-48 that obtains a 3D cubic structure. Moreover, SBA type of MSNs is the more favorite mesoporous particles due to their thermodynamic control mechanism that allows the synthesizing of highly ordered pore size. The SBA (Santa Barbara Amorphous) nanoparticles were first discovered at The University of California, Santa Barbara. The various types of SBA nanomaterials are synthesized for instance SBA-11 (cubic), SBA-16 (cubic-cage-structured), SBA-15 (hexagonal), and SBA-12 (3D hexagonal)[59, 60]. The SBA type nanomaterials have larger pore size and hydrothermal stability than MCM type nanomaterials because SBA type nanomaterials contain the silica walls that their dense are penetrating than MCM type nanomaterials. Furthermore, the desirable types of mesoporous silica nanoparticles are synthesized according to their morphology, pore size by diverse reaction parameters that are catalysis and surfactant types, pH, solvent concentration, and temperature[61]. The strong Si-O bond on the surface of mesoporous silica nanoparticles is stable to external reactions that led to the loading of drug into the pore as a controlled manner. The geometrical parameters such as porosity, pore size, the diameter of MSNs affect the yield of mesoporous silica nanoparticle that is utilized as a nanomaterial of targeted drug delivery mechanism at cancer therapy treatment [62]. Vallet - Reggi et al. studied to inject of anti-

inflammatory drug of ibuprofen into the MSN system according to utilized of high surface to volume ratio and porosity parameters of MSNs[63]. Therefore, porosity, pore size, and diameter of nanoparticle affect the accumulation of MSNs through the blood cells where the cargo reaches to the target tumor tissue as a shorter time. [64].

2.1 Scientific State Of MSN

The discovery of new biological applications needs to understand the diversities of dynamic activities for living systems. Mesoporous silica nanoparticles are plighted to utilize in various bio-applications such as bio-imaging [5], biosensors [6], drug delivery mechanisms [8], gene delivery [11]. MSNs promise the high surface to volume ratio, highly- ordered pore size, low toxicology in living systems, and porosity that feasibilities of MSNs made them good biodegradable material for targeted drug delivery applications. Moreover, the surface modification of MSNs is synthesized easily by the various way in the laboratory environments. Therefore, the physical features of MSNs are developed for synthesized of desirable nanomaterial for varieties applications. Moreover, cell-targeting and cellular uptake are predominant keys for being successful in the drug delivery mechanism. Since the physical properties of MSNs, it allows to harmonies with living biological system dynamics. MSNs are a good candidate for cancer treatments to decrease the side effects that come from current therapies[65, 66]. The side effects also decrease healthy cell numbers in living systems. The synthesis of MSNs should be obtained to design only the target cell type characterization. Hence, the request cargo loading amount fits the geometrical parameters of MSNs. Moreover, when the cargo loading-MSNs enters inside of the cell, the release time of a drug is enough to reach the tumor cell without being destroyed. As a result of these features, MSNs should be synthesized by desired surface features for specific target accumulations.

2.2 Targeted Drug Delivery Mechanism

Targeted drug delivery mechanism aims to decrease the side-effects of cancer therapy such as disease metastases, chemo/radiotherapy, and the growth of second primary tumors. The utilize of MSNs allows minimizing the side-effect of current cancer

treatments. Moreover, the physicochemical properties of nanoparticles which are the size of the nanoparticle, porosity, surface charge, pore size, surface modifications affect the yield of targeted drug delivery mechanisms during MSNs accumulations into the biological system.[67] The surface hydrophobicity and charges are the predominant parameters for avoiding the agglomeration of MSNs during accumulation into the blood vessels [68]. Generally, positively charged of MSNs are more uptake from the tumor cell. Transportation of nanoparticle is divided into two types, which are endocytosis and exocytosis, through the living tissue. According to tissue types, various particle sizes of MSN are utilized for the effect of cellular internalization. However, 100 nm of MSNs are shown better internalization with tumor cells. Moreover, the shape of nanoparticle starts to be a significant physicochemical key when the particle size is more than 100 nm.[69, 70] Targeted drug delivery mechanism contains four steps to succeed on MSNs which bind with negatively charged of glycoprotein (glycocalyx) on the cell that helps to recognize the suitable matter for cell, interiorized of targeted MSNs into the bilayers, endosomal escape step, and MSNs -encapsulated cargo localization on target cell[71]. Moreover, the designing of various targeting nanostructure is a predominant factor to increase the yield of cellular uptake mechanisms during targeted drug delivery. Two synthesis types of targeting nanoparticle, which is active and passive targeting, are utilized for the development of drug delivery mechanisms that need to release the exact amount of drug into the cell without loss from cargo injection during the preparation of MSNs. The working principle of passive targeting agent is to Enhanced Permeability and Retention (EPR) hypothesis. The EPR effect was discovered firstly by Matsumura and Maeda. EPR effect is predominant on the nanoparticle that a certain size of attachment to the tumor[36]. Moreover, different localization of macromolecules is combined with the physiochemical features of certain size nanoparticle which are hydrophobicity, surface charge, and morphology for binding with tumor cells. According to the high yield of the EPR effect, the doxorubicin and temozolomide are loaded as therapeutic agents into the MSNs, immensely[72]. In contrast to passive targeting agents, active targeting agents are obtained by surface modification on the MSNs. The studies showed that cellular uptake time decreases of cancer cells by increases the active targeting agents when the surface of silica nanoparticle folded by folic acid[73].In specific cancer treatments works, such as breast and lung cancer cells absorb the drug-loaded mesoporous silica nanoparticle are functionalized with active charge groups, less time than unfolded MSNs[74].

On the other hand, the main drawback of MSNs in targeted drug delivery applications is to endosomal escape. Because, when the MSNs are accepted into the cell, the cell perceives them as a strange material. Therefore, the digestive enzymes attack MSNs into the endosome for the degradation of nanoparticles with cargo loaded microenvironment. Scientists create the strategies that surface charged behavior of nanoparticle influences the endosomal escape yield. Generally, the negative anion number affects the osmotic pressure of the endosome environment. Therefore, the nanoparticles are escaped from the endosome by swelling effect. Previous studies obtained when the concentration of Cl^- ion increases in the endosome, the cargo loaded nanoparticle can easily run from endosome to cytosol. This strategy is named as a proton sponge effect [32].

According to literature; surface charge properties, electrokinetic potential behavior, surface modification, porosity, and pore size are important for targeted drug delivery mechanisms when the mesoporous silica nanoparticle is utilized. The surface characterization and chemical environment decide the exact drug loading capacities of MSNs as efficient features [75] The stability and dispersion of nanoparticle into the living organism is the key to being successful in entrapped of the nanoparticle by the tumor cell. Understanding the geometric, physical, and chemical mechanism of mesoporous nanoparticle provides achieve targeted drug delivery mechanism in cancer treatment.

2.3. Pore Size and Porosity Effect

The geometric properties of mesoporous silica such as porosity and pore size allow deciding the drug that is chosen for loaded into the pore of MSNs. The internal structures of MSNs decide the cellular uptake process of the targeted drug delivery mechanism [76]. The pore size and porosity parameters are found out the physical effect on the surface of silica nanoparticle. The physical effects cause deviations of surface charge density and electrokinetic potential behaviors[77]. Therefore, the MSNs starts too far away from their equilibrium ionic environments. The controllable drug release rate cannot be predicted when the local variations demonstrate on the surface of the MSNs system. Moreover, the internal structure of MSNs increases the efficiency of drug-loaded into the porous media. The studies discovered that honeycomb structure is the more internalized from the glycocalyx negative charged cellular recognition molecules[4]. The

drug release kinetics are investigated by the porosity parameter. Hence, drug diffusivity and drug release media efficiency are related to the porosity and pore size values.[78, 79]The initial uncontrolled drug loading into the MSNs gets exploring when the porosity and pore size parameters are known by scientists. Moreover, the accumulation time can be estimated through the blood vessels movement to MSNs when the pore size and porosity parameters of nanoparticles are cognized [80]. Furthermore, the large pore sizes of MSNs allow being encapsulating of small molecules, in vivo environment[81]. Current studies aim to synthesize the monodisperse silica nanoparticle that particle size range between 50 to 200 nm with large pore size value (H is more than 5 nm) for encapsulation of high weight biological molecules such as proteins[82, 83]. Hence, previous studies showed that a decrease of particle diameter and pore size caused to development of drug release into the cell – nanoparticle interactions. Yu's group found out that the porosity, surface charge property, and silica toxicology relate to each other. The toxicology level decreases during the cellular interaction between the silica nanoparticle and erythrocyte hemolysis [84]. Finally, Gu et al. synthesized to large pore size (13-24 nm) MSNs that allow showing high adsorption capacity of DNA[85].

2.4. Surfactant Effect

The avoid of agglomeration ensures that accumulation of MSNs without fluctuation into the blood vessels. The cargo- loaded MSNs are stored by proper sample solution for drug carrier mechanism. The stability and dispersion degree of nanoparticle aid to be succeeded in the mechanism that reaches nanocarriers to target tumor cells. Moreover, the surface modification needs for the internalization process during the cellular uptake mechanism. Because the surface modification provides the change in the surface ionic charge environment for both drug- MSNs and MSNs-cell interactions. Micelle and surfactant samples promise to bio-functionalized the surface of silica nanoparticle [86]. Moreover, the chemical properties of a surfactant such as steric hindrance repulsive force, molecular weight, viscosity, graft density affect the stability of the nano carrier[87]. Hence, the specific surfactant salt molecules ensure to MSNs as the salt effect. The salt effect focusses on the thickness of EDL on the surface of MSNs where provide the stability of silica nanoparticles into the sample solvent. Generally, the hydrophobic surface of nanoparticle becomes hydrophilic when the surfactant is used for

stabilization. The repulsive force between the nanoparticle is created by zeta potential where the local surface charge variation is obtained on the surface of the silica nanoparticle system. Jiang et al. studied that surfactant usage affects the repulsive force on the silica nanoparticles and eliminate the Van der Walls force attraction [88]. Moreover, the monodispersity of silica nanoparticle is increased by the utilization of surfactant. The most popular surfactant is sodium dodecyl sulfate (SDS), oleic acid, polyvinylpyrrolidone (PVP), and polyacrylate (PA)[89, 90] The selection of the right surfactant is predominant for the stabilization of nanoparticle into the sample solution. The main drawback of the utilization of surfactants is the high-temperature environment. When the temperature rises above the 60 Celcius, the viscosity of the surfactant is damaged[91]. However, Shahrul et al. developed the strategies that decrease to temperature effect on zinc (Zn) nanoparticle [92]. Previous studies showed that the surface modification of MSNs with PA surfactant increased the encapsulation of drug nano-carrier during cellular uptake mechanism [93, 94]. Moreover, the hydrophobic properties of mesoporous silica nanoparticle allow modifying with PA surfactant less time than other surfactant samples. Also, utilization surfactants should be cost-effective. Because the experimental procedures always are developed according to literature searches and experience into the laboratory.

In conclusion, the surfactant utilization directly relates to the surface charge density of mesoporous silica nanoparticle and EDL. Therefore, the knowledge about surface charge characterization of MSNs helps to understand the design whole mechanism through the targeted drug delivery in cancer treatments.

2.5. Surface Charge and EDL Effect

The ionic environment of the aqueous media interaction with the solid surface is caused to surface charge on the silica nanoparticle. The protonation/ deprotonation chemical reactions occurred during a solid/liquid interface. The change of pH, monovalent anion/cation number, and ionic distribution affect the surface charge behavior of the solid interface. The repulsion force between co-ions and attractive force between counter-ions are formed by Electric Double Layer (EDL) on the surface of the nanoparticle. The growth type of EDL decides the surface charge behavior of nanoparticle. Hence, ionic concentration affects the EDL growth type. Therefore, surface

charge and EDL are thought together when the characterization of the nanoparticle is obtained. The Boltzmann-Distribution explains the behavior of the nanoparticle surface. This distribution is simplified by these assumptions: the zeta potential magnitude is lower than 25 mV, the surface must be flat and enough to far away from any other bodies. The electrokinetic behavior is calculated as an analytically by utilization of the Poisson-Boltzmann model. However, the mesoporous system cannot be explained by Boltzmann-Distribution and Poisson Boltzmann model. Because, when the EDL develops on the surface of a silica nanoparticle, the thickness of the ionic layer will decrease, and the opposite surface of nanoparticle will overlap with their EDL. The overlap on the surface of the nanosystem causes the local variations on the surface charge. Therefore, Poisson-Boltzmann modeling will be invalid. In real-life applications, the flat surface assumption cannot give the correct behavior of the surface charge. Moreover, previous studies applied the PB modeling for ignored these facts where the applications were focused on the nano-system in literature[42, 44]. The different sizes and internal structures are synthesized in a laboratory environment in current studies. The physical effects are developed on the surface of the nano-system such as EDL, curvature effect. Therefore, these physical effects cause to the development of new nano-system modeling for analytical measurements. Hence, the ionic distribution will be different than BD assumptions under the surface of the nano-system.

In the mesoporous silica nano-system, the geometrical properties lead to creating a different behavior on the surface pore opening and the total solid surface. The ionic distribution will avoid explaining by Boltzmann Distribution according to mesoporous silica designs. The size of the particle and ionic concentration effect on the demonstration of EDL overlap. Moreover, the curvature effect on silica surface is obtained by the decrease of the surface to volume ratio of MSNs[54, 95]. Therefore, the flat surface prediction will not be demonstrated according to mesoporous silica nanoparticle geometry.

On the other hand, the Nernst-Planck equation provides the display of the ionic distribution of the mesoporous nanosystem. Hence, the Poisson equation shows the electric distribution on the silica surface. Poisson-Nernst-Planck (PNP) equation combines for calculating electric distribution was formed to the EDL on the mesoporous nanoparticle. The nano-system surface charge characterization on the nanoparticle must be solved by the utilization of the PNP equation without Boltzmann simplification.

2.6. PNP and Charge Regulation Model

Generally, the constant surface charge and constant potential are utilized as boundary conditions for calculation both analytical and numerical solutions of PNP equations. However, the electric surface charge and electrokinetic potential demonstrate the variation in real surface physics effects. The surface charge occurs on the nanosystem when the protonation/ deprotonation reactions create the electrical charge because of solid/liquid interaction. Therefore, the ionic distribution demonstrates the function of surface charge and these two physics should be solved by the PNP equation with a Charged Regulation model. This modeling is started to use in the mesoporous nanoparticle system as a boundary condition for an exhibition of surface interactions both nanoparticle and their interaction with other species. The explanation of surface charge behavior is invalid with the utilization of boundary conditions that are constant potential and surface charge density.

The Charged Regulation Model was created by Ninham and Parsegian in the literature, firstly [53]. In numerical studies, Charge Regulation Model has been investigated for the active charge model as a boundary condition of surface characterization. The electric double layer effect finds out by Charge Regulation in various application areas which are colloidal chemistry, atomic force measurements (AFM), ion adsorption [96, 97]. The characterization of the colloid system and AFM studies explain with Charge Regulation Models [98, 99]. The physical effect on the nanoparticle such as EDL overlap explains by the Charge Regulation concept. The EDL effect strongly relates to the pH and ionic distribution of the colloidal environment. This solid/liquid interaction demonstrates the variation on the local surface charge density in diverse EDL ionic conditions. Previous studies about force measurements with surface forces apparatus (SFA) are impacted by the Charge Regulation model [100, 101]. These studies focused on the flat surface of surface charge during the force measurement application with the known surface location. In literature searching, there is no proper information about surface charge behavior of mesoporous silica nanoparticle. In colloidal stability and dispersion applications, the surface charged density gives information about local ionic distribution on the surface of nanosystems. In our study, the CR Model used as a boundary condition of the surface. The analytical solution of electric potential characterization was found by multi-ion active CR modeling.

The surface charged density of the curved geometric shape of mesoporous silica nanoparticle and deprotonation/ protonation reaction on the surface of MSNs are calculated by Charge Regulation. Moreover, surface charge characterization of nanochannels is investigated by diverse studies of CR Model [102, 103]. However, there is less information and analytical solution studies about electric potential identification on the mesoporous silica nanoparticle in the literature. Furthermore, the colloidal interaction of spherical particles was explained by the theory of Derjaguin, Landau, Verwey, and Overbeek (DLVO) in experimental studies that van der Waals and electric double layer forces are predominant in this theory. When the EDL overlaps occur on the nanosystem by the diversity of ionic environments, The Charge Regulation model needs to use as a boundary condition that solved together with the PNP equation in the nanosystem.

CHAPTER 3

EXPERIMENTAL MODEL

The dispersion and stabilization of silica nanoparticle are critical points for the demonstration of the yield in the colloidal nanofluids. The amorphous silica nanoparticle only contains silanol functional groups (SiOH) on the surface of the nanoparticle. The stabilization of small nanoparticles is lower than large nanoparticles because of the effect of the surface to volume ratio on the nanoparticles. Therefore, the hydrophilic properties of silanol groups eager to aggregate together into the water solution or solutions where include the high percentage of water content. The precipitation of silica nanoparticles is easily recognized because of the gravitational force. The agglomeration occurs when the attractive force is more predominant than the repulsive force between the nanoparticles. The agglomeration causes the accumulation of problems through the application process of the nanoparticle. The characterization of nanoparticles is a major phenomenon for estimation of utilization yield in application processes. Therefore, the size and zeta potential measurements are applied to the silica nanoparticles that are produced in various sizes. The particle size and zeta potential measurements give a clue about the stabilization of the silica sample. The adjustment of pH, chemical behavior of solvent, monovalent cation salt concentration, and nanoparticle amount need to investigate for decided to stabilization degree of nanoparticles.

3.1. Particle Size Measurement

The most common analysis that finds out the particle size is DLS (dynamic light scattering) method. Small nanoparticles randomly undergo the thermal motions that are explained by Brownian motion. The working principle of the DLS method is to measure the particle size according to the Brownian motion of nanoparticles that depends on their sizes[104, 105]. The laser beam is hit the sample and the scattering light reflects by Θ degree. The intensity of light difference from entrance to exit is used to measure the wave vector (q) which is utilized for correlation factors that give the particle size distribution of decay times. In equation 3.1 demonstrates the wave vector calculation. In equation 3.1.

q refers to wave vector, θ refers to scatter angle, λ refers to wavelength, and *n* refers to refractive index. Next, the average particle size is solved by the Stokes-Einstein equation. In equation 3.2, D_h refers to the hydrodynamic diameter, D_t refers to the translational diffusion coefficient, k_B refers to Boltzmann's constant, T refers to thermodynamic temperature, and, Ƞ refers to dynamic viscosity, and D_t refers to the diameter of the colloidal particle. The Stokes-Einstein equation is solved by the instrument software. Also, the light source is a laser light that signals hit the solution at 90 degrees through the detector. The refractive index and viscosity of liquid solvent are entered for getting the particle size results. In figure 3.1 displays the schematic illustration of the working principle of the DLS method.

Moreover, the solvent type is an important parameter for the DLS method that gets the correct result from analyses. Therefore, the surfactant salts are utilized as a polar solvent. As previous studies, an ammonium salt of polyacrylate surfactant (PA-NH_4) is used as a dispersion material for silica nanoparticle because of their anionic surface charge[89, 91]The dose of surfactant increases the repulsive force degree between nanoparticles for avoiding the fluctuation. Moreover, the steric repulsive force of polymeric dispersive solution causes to increase in the total surface charge of the colloidal system. Hence, D_h is influenced by the ionic environment of the colloidal sample solution.

$$q = \frac{4\pi n}{\lambda} \sin\left\{\frac{\theta}{2}\right\} \tag{3.1}$$

$$D_h = \frac{k_B T}{3\pi \eta D_t} \tag{3.2}$$

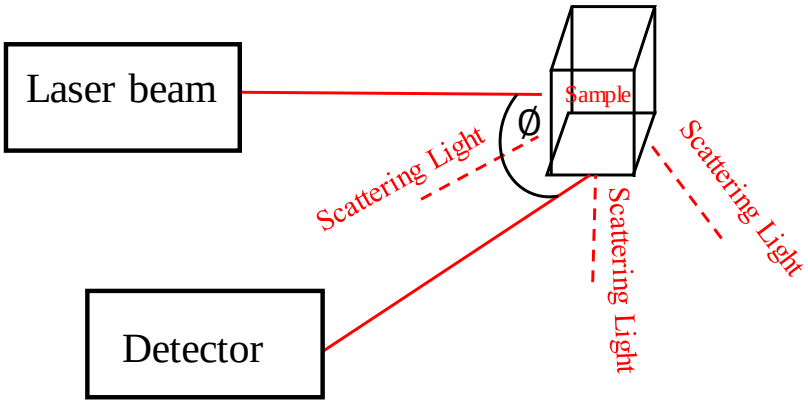

Figure 3.1. Schematic illustration of the DLS (direct light scattering) method.

The adjustment of pH, silica amount in the solution, ultrasonication, monovalent cation concentration, and volume of surfactant are predominant factors for the development of dispersion of silica nanoparticle into the sample liquid. The dispersion of nanoparticle is managed by breaking the bonds where lead to agglomerate into the solution.

The Ultrasonication process is applied to the silica nanoparticles that provide stability to the ionic environment. In the literature, there is no evidence to avoid the agglomeration of silica nanoparticles that are exposed to a longer time to the ultrasonication process[106]. Because each silica nanoparticle solution needs to investigate their own optimum duration time for learning of their ultrasonication process. Yang et. al. discovered that the optimum duration time is a maximum of 30 minutes for water medium silica nanoparticles [107]. Therefore, ultrasonication applied to the nanoparticles between 20-30 minutes during our experimental procedures.

Firstly, the DI is selected for various sizes of silica nanoparticles as a solvent. The silica nonporous nanoparticles were bought from EVONIK company. The silica nanoparticles have various sizes and surface areas. The names of particles are Aerosil 90, 150, 200, and OX50 and TT600. In literature, the most commonly utilized particles are Aerosil 200, 90, and OX50 of fumed silica nanoparticles. All amorphous silica nanoparticles are produced by silanol groups. The protonation/ deprotonation reactions on the surface of silanol groups affect the stability of silica nanoparticle. The pH of the solution and ionic distribution controls the dispersion factor of the silica nanosystem. Therefore, in the previous study demonstrated that the adjustment of pH was kept at 8 for better dispersion[108]. According to that, the first experiment is decided to effect of pH on the silica nanoparticle solution. The adjustment of pH is utilized by 0.1M of NaOH.

After, as mentioned before, the 75-150 ppm amount of silica nanoparticle was dispersed into the DI water[109]. Therefore, the silica amount range was kept constant into the water solvent. Moreover, the monovalent cation (Na+) was used as a control of repulsive forces between nanoparticles. The monovalent cation decides to the thickness of the EDL on the surface of the nanoparticle. When the number of monovalent cations increases, the development of EDL increases, as well. The DLS method was used for particle size analyses. Also, the zeta sizer nano instrument software is used for the measurement of the Stroke-Einstein equation. In the DLS method, the refractive index of water is 1.33, the viscosity of water is 0.890 cP at room temperature. Aerosil 200 (12 nm) and Aerosil 90 (20 nm) are used as silica nonporous particles.

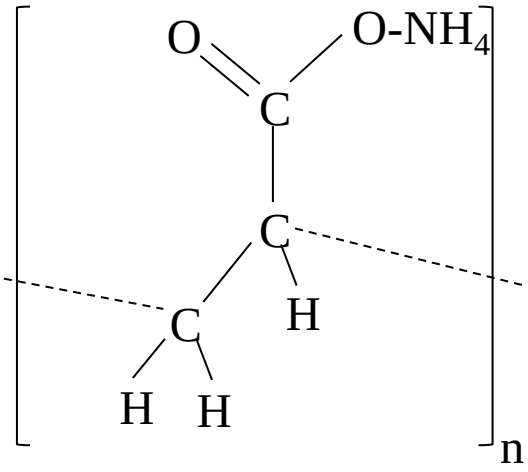

Figure 3.2. Schematic illustration of the ammonium salt of polyacrylate polymer (APA)

Other steps are to establish the surfactant effect for particle size measurements. The figure 3.1 exhibits to the chemical functional groups of NH4-PA (APA) surfactant salt. The APA surfactant reacts to the silanol group of the surface silica. The surface modification allows increasing the dispersion of silica nanoparticle into the surfactant solvent. Therefore, the agglomeration ratio decreases when the anionic solvent is used for stabilization. In the DLS method, the refractive index of the APA solvent was 1.5, the viscosity of the APA solvent was 1 cP. Firstly, the different volumes of the APA solution are poured into the silica nanoparticle. Aerosil 200 (12 nm) is used as a silica nonporous particle. The result was recorded from instrument software. Next, the silica amount is decided to understand the saturation level of silica nanoparticle into the APA solvent. Therefore, various amount of Aerosil 200 silica nanoparticles are poured into 4.5 ml of APA solvent at pH 8. The adjustment of pH was done by 0.1M NaOH. Each solvent has

its saturation degree ratio for the solute. Therefore, silica nonporous particle was shown different solubility and stability into the APA solution.

Furthermore, another particle size determination method is the Scanning Electron microscope method (SEM). SEM is used for diverse applications such as topography, morphology, composition, and crystallographic information about nanosystems. The resolution degree of SEM analyses is around 30 nm. The working principle of SEM is to interact with electrons with the specimen and generate a variety of signals. The SEM analyses allow imaging large amount of sample as a scale-up model in a 2D sample of the line by line. Hence, electrons are used to get the imagination process. The electron beams are focused on the sample by the optic lens. After that, electrons are hit the sample and detectors collect the reflective lights from the sample. Also, the SEM analyses are done under vacuum conditions. EDT detector is used for SEM measurements in our analyses. Moreover, both dry fumed silica and liquid silica sample are utilized for SEM experiments. The pH was adjusted at 8 and the DI water was used as a solvent. Ultrasonication is applied to each liquid silica particle solution for around 30 minutes. For dry and liquid silica nanoparticle, each sample put into the oven for 2 hours at 115 Celcius that is avoided from moisturizing effect before the SEM analyses.

3.2. FTIR Measurement

FTIR analyses focus on the polar covalent chemical bond interaction into the solution. Therefore, FTIR is used to characterize the chemical environment of the nanoparticle. Each chemical bond vibrates its special wavelength. The stretching of each polar bond provides to characterize the chemical functional groups of unknown or known samples. The working principle of FTIR is to detect that stretching's which are absorbed from nanoparticle samples between the infrared light region. The APA surfactant was utilized as a solvent by each analyst. surface modification on the surface of silica nanoparticle is showed by FTIR results. The results are read both in air and solvent. Taken solvent type data from instruments aim to eliminate the moisturize stretching wavelength from water. The absorbance versus wavelength data is collected from FTIR instruments. According to the absorbance graph, the strengths of the polar bond are identified in silica samples.

3.3. Zeta Potential Measurement:

The total surface charge is the evidence of colloidal stability and equilibrium of the nanoparticle system. Surface charge variations affect the EDL of the nanoparticle. The zeta potential measurements allow getting information about colloidal stability. Zeta potential is the electrical potential that exists between the Stern layer and EDL. The magnitude of zeta potential is indicated the potential stability of the nano-system.

$$\mu e = \frac{\varepsilon \zeta}{\eta} f(\kappa R_s) \tag{3.3}$$

The determination of zeta potential measurement is applied to Henry's law (3.3) by the instrument software. The μ_e refers to electrophoretic mobility, ε refers to dielectric constant, ŋ refers to the viscosity of the medium, $f\kappa$ refers to debye function, ζ refers to zeta potential, and R_s refers to the diameter of the colloidal nanoparticle. The zeta potential is measured in aqueous dispersion by PALS (phase analyses light scattering) with used Henry's law. The working principle of PALS is similar to the DLS method. Electrophoretic mobility is measured by the shifting of small frequency because of the light scattering of the laser beam[110]. The small frequency changes allow the mobility of nanoparticle in an external electric field through zeta potential measurement. The zeta sizer measurement of Malvern contains two different electrophoretic mobility measurements to calculates zeta potential value. Firstly, the fast field reversal (FFR) mode is the speedy reversing external field that is utilized to measure true particle mobility without counted the electroosmotic field. Therefore, the average zeta potential value is calculated by FFR. Secondly, slow filed reversal (SFR) mode is the slow reversing external field that decreases the polarization of electrons. Therefore, the distribution of zeta potential value is calculated by SFR.

Moreover, the ionic concentration impacts the EDL thickness on the surface of silica nanoparticle. The salt concentration is the predominant key to measure the zeta potential value for investigation the colloidal stability. Therefore, different salt concentrations are poured into the DI water silica nonporous nanoparticle solutions. As a monovalent cation, the Na+ is provided by NaCl salt. The pH is adjusted at 8 by utilized 0.1 M NaOH during

zeta potential measurements. The value of pH is decided from the experiments of particle size measurement that investigated before. Also, the isoelectric point (IEP) of silica nonporous nanoparticles is close to 2 [111]. Therefore, the IEP point is the reference that justifies the pH range during experimental procedures. All experiments are done by taking into consideration of IEP of silica.

CHAPTER 4

NUMERICAL MODEL

4.1. Theoretical Background

The solid surface interaction with ionic media creates the chemical reactions which are named as an association/ dissociation on the solid/liquid interface. The aasociation/ dissociation chemical reactions change the total surface charge on the solid because of the attractive and repulsive forces between the SiOH groups on the solid surface and co-ions. The ionic distribution occurs on the surface of the solid system. This ionic distribution is explained by Boltzmann Distribution. The Poisson-Boltzmann (PB) equation is demonstrated to calculate the electric potential distribution through the electric double layer in the nanosystem by analytically. The Debye- Hückel simplification allows us to solve the PB equation for calculation of the electric potential of surface that magnitude is lower than 25 mV. However, Boltzmann Distribution has limitations that applied on the charged surface. These limitations are to surface must be flat and adequately away from any other surface, the electric potential of the surface must be lower than 25 mV, and EDL on the surface is developed as an extended infinitive. PB equation is not utilized when opposite surfaces are close with each other that their EDLs are developed to opposite surfaces where starts to overlap, the local ionic distribution displays the variations. Hence, EDL overlapping case occurs the difference of electric potential through the surface of nanosystem than non-overlapping case so, Boltzmann Distribution has demonstrated the deviation when the EDL overlap is predominant on the surface of the nanoparticle. Therefore, the Poisson-Nernst-Planck (PNP) equation is used for correctly solved on the surface of electric potential distribution. PNP equation calculates the ionic mass transport when the EDL overlapping case is created on the surface of the nanosystem. In equation 4.1 and 4.2 display the PNP equation where are solved analytically. Moreover, the boundary conditions are set for correct calculation on the surface as an analytically. In the literature, constant surface charge or constant potential is utilized as a boundary condition where the PNP equation is applied on the surfaces of the system[112-114]. The real physics of the surface are not explained

correctly when the boundary conditions are set as a constant surface charge or electric potential.

$$-\varepsilon_0 \varepsilon_r \nabla^2 \psi = F \sum z_i c_i \tag{4.1}$$

$$\nabla . \vec{N_i} = \nabla . \left(-D_i \nabla c_i - z_i \frac{D_i}{RT} F c_i \nabla \psi \right) = 0 \tag{4.2}$$

The EDL overlap causes the deviation of the electric potential value at the surface of the particle when the constant surface charge density is predicted on the surface of the nanosystem. The same behavior is observed when the constant electric potential is assumed on the surface, the variation on the surface charge density demonstrated on the surface because of the EDL overlap issue. The non-uniform ionic distribution on the surface of nanoparticle is caused to solve the PNP equation correctly in real physics by using constant surface density and electric potential as a boundary condition. Moreover, the surface charge and electric potential show the variance behavior because of the local ionic distribution. Therefore, the charge regulation model needs to apply to our system for the elimination of these variances. The charge regulation model is created according to variation of surface charge with surface chemical reactions, adsorption of ions, and electrolyte solution conditions. The charged regulation model is applied on the surface of the nanoparticle and their interaction with each other for solved the PNP equation properly with boundary conditions.

In our study, a mesoporous silica nanoparticle with various diameters, porosity, and ionic concentration structure on its surface is considered. The aqueous media is considered as KCl (i.e. symmetric 1:1) electrolyte solution that contains 4 type ionic species which are named as H^+, K^+, Cl^- and OH^- ions with their bulk values being c_{10}, c_{20}, c_{30}, and c_{40}, respectively. When the silanol groups on the surface of silica nanoparticle react with KCl solution that contains ionic species, the surface on silica nanoparticle becomes to charge due to the association/dissociation chemical reactions. The larger ions which are K^+ and Cl^- mostly dominate the surface charge and the pH value of the solution is decided by the numbers of H^+ and OH^- ions.

Two fundamental dissociation/association reactions take place in the solid/liquid interface during this chemical reactions:

$$SiOH \leftrightarrow SiO^{-} + H^{+} \tag{3.2}$$

$$SiOH + H^{+} \leftrightarrow SiOH_2^{+} \tag{3.3}$$

The equilibrium constants are calculated by using:

$$K_A = \frac{\Gamma_{SiO^-}\left[H^+\right]_w}{\Gamma_{SiOH}},\ K_B = \frac{\Gamma_{SiOH_2^+}}{\Gamma_{SiOH}\left[H^+\right]_w} \tag{3.4}$$

In equation 3.4, Γ_{SiO^-}, Γ_{SiOH} and $\Gamma_{SiOH_2^+}$ are the surface site densities of SiO^-, SiOH, and $SiOH_2^+$, respectively, and $\left[H^+\right]_w$ is the hydrogen concentration at the solid/liquid interface. The surface charge density of the silica surface is solved by:

$$\sigma_w = -\frac{F\,\Gamma_{total}}{N_A}\frac{K_A - K_B\left[H^+\right]_w^{\,2}}{K_A + \left[H^+\right]_w + K_B\left[H^+\right]_w^{\,2}} \tag{3.5}$$

4.2. Numerical Model

In this part, the numerical model and the creation of a geometric model will be explained. In figure 4.1 (a.-d.) demonstrates the schematic representation of the numerical study. In this study, the specific mesoporous silica nanoparticle which is Santa Barbara Amorphous-16 (SBA-16) [] is designed by COMSOL. In figure 4.1 a. the part is displayed to shape SBA-16 nanoparticle that is done in a laboratory at highly ordered porous geometries. In the figure, 4.1-b demonstrates the linkage type of SBA-16 nanoparticle. In the figure, 4.1-c shows the geometrical execution of mesoporous silica nanoparticle in the 2-D cartesian system.

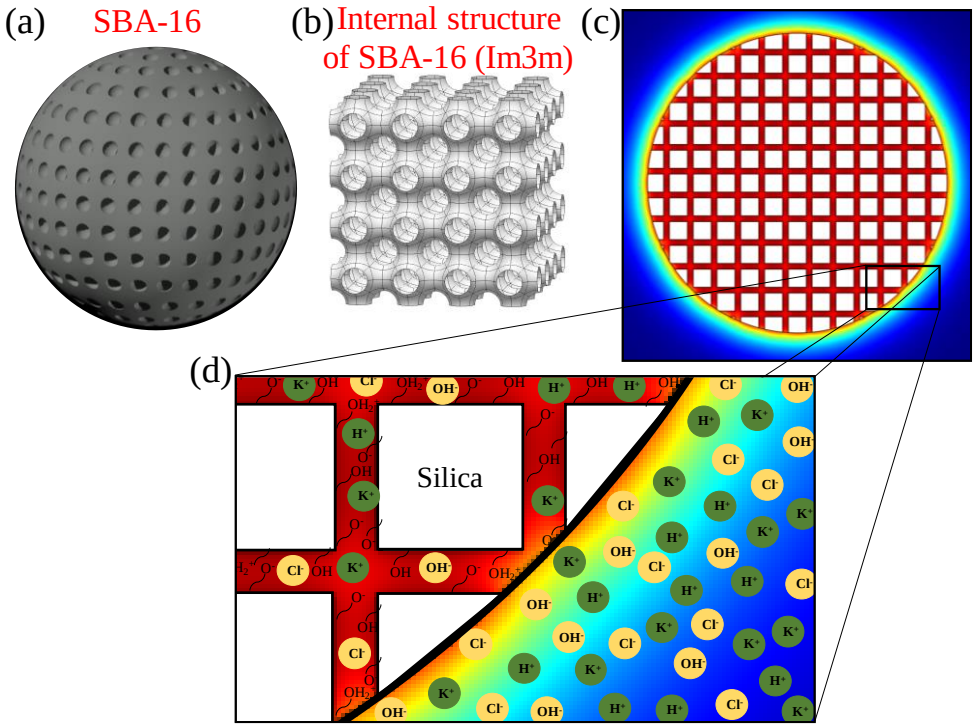

Figure 4.1. (a-b) Representation of geometrical structure of the mesoporous nanoparticle (c-d) Schematic representation of the numerical model.

Mesoporous silica nanoparticle contains the silanol (SiOH) groups on the surface. The surface reacts to change in the surface total charge into an ionized liquid. The liquid phase contains the neutral KCl salt with the bulk concentration of C_{KCl}. The KCl salts are ionized with adjusted to the pH of the electrolyte solution by utilized KOH and HCl. There are four ionic species (i.e., N = 4, H^+, OH^-, K^+, and Cl^- dissolved in the solution.)

Ci_0 is the bulk molar concentration of the i^{th} ionic species and C_{i0} of each species satisfies the electroneutrality condition:

$$C_{10} = 10^{-pH+3} \quad C_{40} = 10^{-(14-pH)+3} \qquad (\text{pH} \le 7) \tag{4.1}$$

$$C_{20} = C_{KCl} \qquad C_{30} = C_{KCl} + C_{10} - C_{40}$$

$$C_{20} = C_{KCl} - C_{10} + C_{40} \quad C_{30} = C_{KCl} \qquad (\text{pH}>7) \tag{4.2}$$

The electrostatic potential variation on the surface of mesoporous silica nanoparticle is designed by the multi-ion charge regulation model[45]. Poisson-Boltzmann, and Nernst- Planck equations explain the ionic mass transport, distribution of electrostatic potential on the surface of mesoporous silica nanoparticle. The charge regulation model is utilized as a boundary condition with these two equations for characterizing the surface charge behavior of nanoparticle. Equation 4.3 is calculated the surface charge density of a nanoparticle surface:

$$\sigma_w = -\frac{F\,\Gamma_{total}}{N_A}\frac{K_A - K_B\left[H^+\right]_w^{\,2}}{K_A + \left[H^+\right]_w + K_B\left[H^+\right]_w^{\,2}} \tag{4.3}$$

Equation 4.1 demonstrates the hydrogen concentration by used equation 4.3. The hydrogen concentration is updated with each numerical measurement. The next iteration has used these results. Therefore, the ionic concentration and electrical potential are solved in each cycle simultaneously. The total surface charge of silica nanoparticle depends on the alteration of the bulk concentration of the ions. The alteration on the bulk concentration occurs to change of pH and local ionic salt concentration of the solution. As a result, the iterative finite procedure is used to measure of surface charge density of mesoporous nanoparticles.

4.3. Computational Details

Firstly, the boundary conditions are applied on the computations. PNP equation in 2-D cartesian coordinates solved analytically using COMSOL Multiphysics software through the solution of equations where the Finite Element Method was employed. The finite element method provides to a certain number, distribution, and shape of the computational elements. The mesh independence test was applied to the finite element method by worked the optimum mesh case. Different mesh densities are employed for extended the mesh independency. Finer mesh adopted a close region to the EDL and surface of the nanoparticle. Physical parameters used in the simulations are; $\varepsilon_0\varepsilon_f = 7.08\times10^{-10}\,F/m$, $R = 8.31\,J/(mol\times K)$, $F = 96490\,C/mol$, $T = 300\,K$, $N_{total} = 4.86\ sites/nm^2$, $pK_A = -\log K_A = 7$ and $pK_B = -\log K_B = 1.9$.

To validate the current model simulations were done at certain numerical analyses environment (C=50 mM, Dp=9 nm, pK_A=7.0, pK_B=1.9, N_{total}=4.75mol/m^2) [115] .The results were compared with experimental data that exists in the literature [55]. In Figure 4.2 experimental data and numerical data show the same agreement with each other.

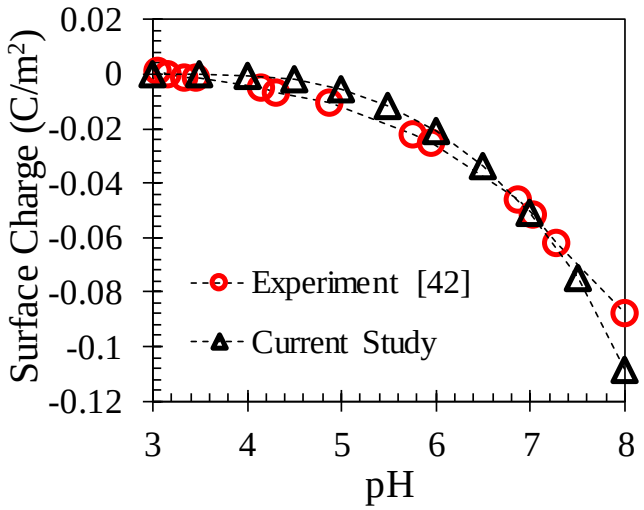

Figure 4.2. Surface charge densities outside mesoporous silica. Black markers indicate the numerical results while the red markers are the results of the experimental results.

In figure 4.2, the validation that was given the numerical procedure presents problems solved by COMSOL Multiphysics software using the finite element method. The liquid phase is KCl as in our previous study for verification of the numerical analyses. The silica nanoparticle was designed as a non-porous silica surface at D_p= 9 nm and put into an electrolyte solution (KCl). The numerical data were measured and compared with experimental surface potential values which were taken from the literature [55].

As a result, in the figure of our numerical data displays a good agreement with experimental values obtained from the experimental surface charge measurement literature.

CHAPTER 5

RESULTS

5.1. Numerical Results

This chapter aims to describe that mesoporous physical parameters were established with porosity (ϵ), pore size (H), and solid perimeter with an applied various diameter of MSN and different ionic condition environments by numerical solution technique. The illustration of physical effect eliminations applied both large ($D_{Particle}$=330 nm) and small ($D_{Particle}$=50 nm) diameters according to their various porosities (ϵ) and pore size (H) values.

Figure 5.1 explains the local zeta potential (ζ_{local}) variations of numerous pore size values (H=5,8.5,11 nm) at the constant 2D porosity value (0.166) and thin EDL thicknesses (λ = 0.97nm) on the 330 nm MSNs, where the ionic environment molarity was C_{KCl}=100mM. The upper side of Figure 5.1 represents to electric potential contours of each MSNs. The size of the solid pore entrance was kept constant at 81% to stabilize the number of pores for eliminating the physical effects from the geometric shape on the zeta potential value. According to electric potential contours, the EDL overlap was not developed out of the surface since the λ value was lower than the H value. The curvature effect was not growing the outside of pores at $D_{Particle}$=330 nm. Because the solid structure lengths were more than 50 nm, the curvature effect could not create on the surface of the solid structure. The high surface to volume ratio was not permitted to develop of curvature effect on the surface of the particle. According to results, the average magnitude of total local zeta potential decreased when the pore size increased on the surface of the MSNs in 2D H values. Hence, the local variation of zeta potential reached the bulk environment in pores when the pore size increased at the high diameter of the MSN ionic environment such as at H=8.5 nm and 11 nm. The case of H=11 nm demonstrated that the magnitude of the total zeta potential value was equal to zero (mV=0)at the pore throat.H=5 case showed that the EDL overlap started to develop into the pore. Furthermore, the magnitude value of solid zeta potential was examined as close as the zeta potential of flat silica nanoparticle. When the decrease of H was observed, the number of pores on the surface

increased. The increase of surface pore size caused the appears of the corner effect on the surface of MSNs. However, the high H values vanished the corner effect of the pore both external and internal area.

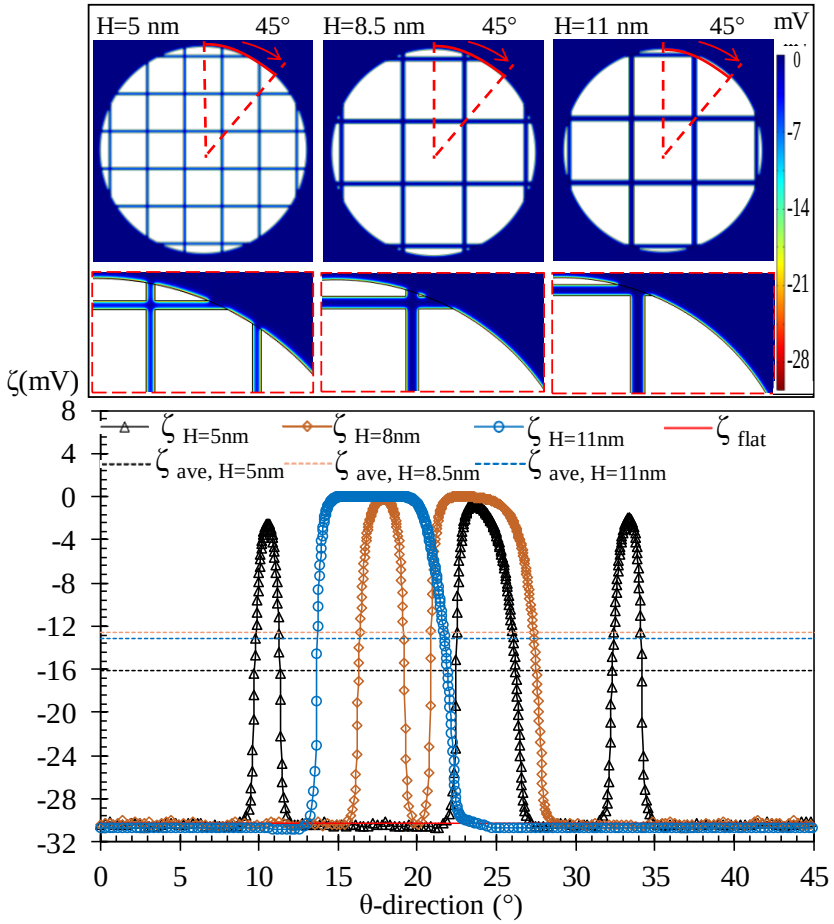

Figure 5.1. a.) Electric potential distributions of different H values at D_p=330 nm and C=100mM. b.) Zeta potential distribution with varying pore size values at D_p=330 nm and H =5 nm, 8.5 nm, 11 nm.

Also, figure 5.2 demonstrates the effect of the different 2D porosity cases on the $D_{Particle}$=330 nm. The $D_{particle}$=330nm were designed on COMSOL at ϵ=0.166, 0.345, 0.47 with ionic environment, C_{KCl}=100mM. To develop the physical effects, where caused the geometric disorders on the nanoparticle, affected wrong local zeta potential calculations on the surface of MSNs.Therefore, the solid structure perimeters were preserved at 81%. According to graphics in Figure 5.2, the average magnitude of local zeta potential increased when the porosity decreased. Hence, the magnitude zeta potential of the solid structure adapted to the electric potential magnitude of flat plate theory. The pore numbers on the surface increased, when the ϵ (porosity) increased the MSNs. The increased of pore structure on the surface of the MSNs, it caused to improve the corner effect on the pore

throat. Hence, both pore entrance and solid structure of MSNs in every porosity are demonstrated similar behaviors because of the same EDL overlap ratio.

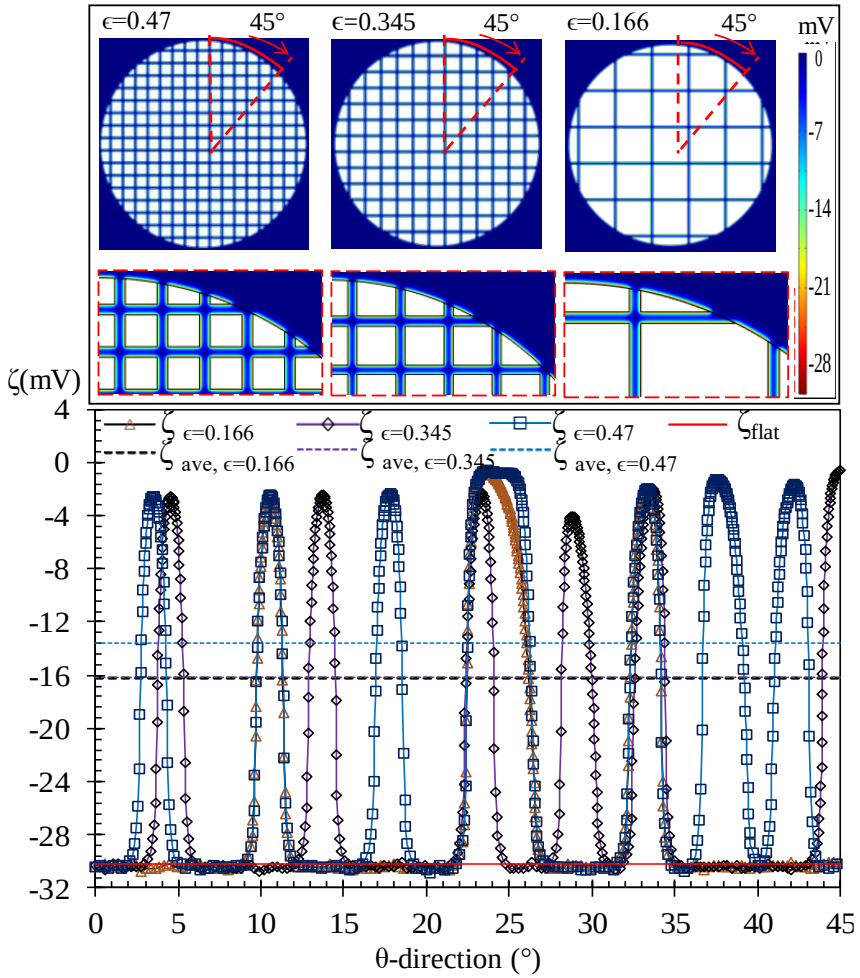

Figure 5.2. a.) Electric potential distributions of different ϵ value at D_p=330 nm and C=100mM. b.) Zeta potential distribution with varying pore size values at D_p=330 nm and ϵ =0.166, 0.345, 0.47.

Moreover, figure 5.3 examines to compare diverse EDL thicknesses on the large diameter of mesoporous systems. Figure 5.3 focuses on understanding the importance of EDL overlap on the zeta potential at MSN. The zeta potential measurement was calculated for four different ionic concentrations by the multi-ion active charge regulation modeling. The all-electric potential contours of the situations were represented in figure 5.3 (a) with their different EDL thicknesses (λ= 0.56,0.97,15.6, 30 nm). The higher EDL thickness created the EDL overlap of the opposite side on the surface of MSNs. Therefore, the EDL overlap caused to observe the significant difference between pore inside and pore throat on the surface. According to results, the average magnitude of zeta potential increased while the EDL thickness (λ) increased (where decreased the concentration) so, higher λ values showed how to affect of EDL overlap mechanism in the mesoporous

nanoparticle. There were seen that the λ=30.6 nm, 15.8 nm created a corner effect on the solid particle of MSN. Also, Figure 5.3 (c) defined the deviations at lower EDL thickness (λ=0.97nm and 0.56 nm) where the local ζ was normalized as a function of flat plate theory. Moreover, the higher values of EDL thickness were developed to discover the corner effect on the solid surface of MSN because of the EDL overlap effect on the pore entrance. Besides the fact that the high ionic environment supplied to reduce of EDL overlap effect on the MSNs.The total zeta potential magnitude reached the zero which meant that the mesoporous nanoparticle system reached the bulk concentration, spontaneously. Furthermore, the (d) part of figure 5.3 demonstrates that the average zeta potential magnitude was normalized by the function of flat theoretical plate calculations. As seen in the d part of figure 5.3, The lower EDL thicknesses showed the behavior far away from flat plate theory estimations.

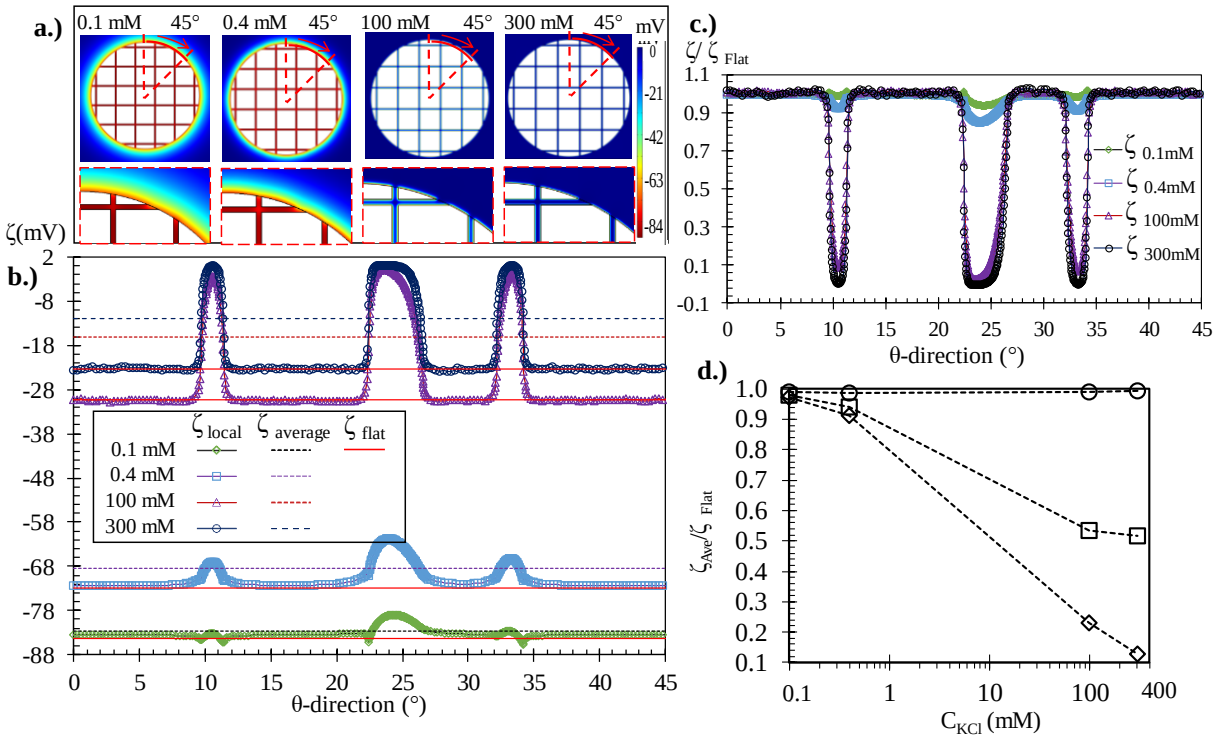

Figure 5.3. a.) The electrical potential response contours through the 45 degrees on the surface of MSNs. b.) Zeta potential distribution with varying ionic concentra. values at D_p=330 nm and λ =30.6 nm, 15 nm, 0.97 nm, 0.56 nm. c.) The local zeta potential normalized as a function of flat theory silica plate. d.) The solid, pore, local zeta potential average value normalized with flat theory silica nanoparticle at λ =30.6 nm, 15 nm, 0.97 nm, 0.56 nm (pH=6).

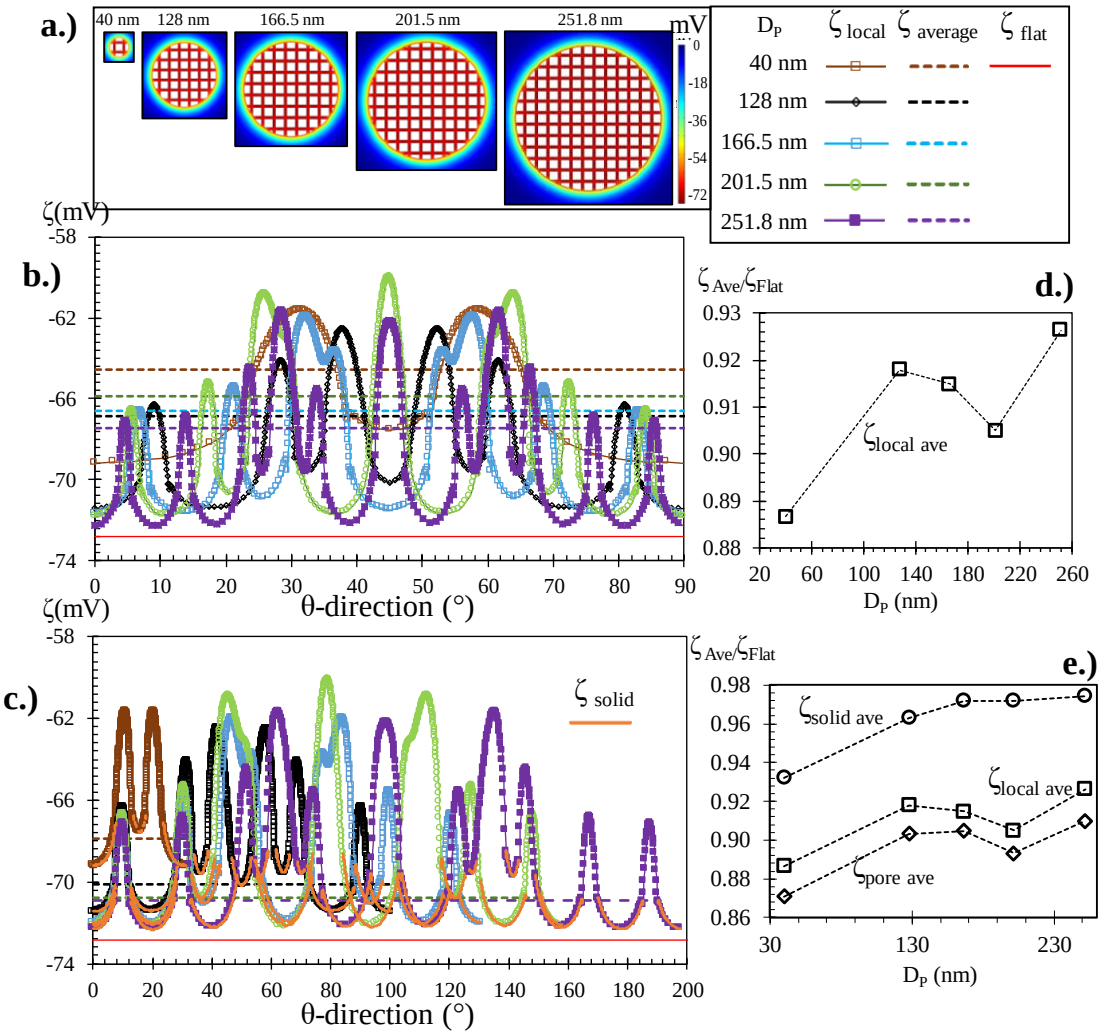

Figure 5.4. a.) The electrical potential response contours through the 45 degrees on the surface of MSNs. b.) Zeta potential distribution with varying diameter values at D_p=40, 128, 166.5, 201.5, 251.8 nm at C_{KCl}=0.4 mM c.) Zeta potential distribution with varying diameter values at D_p=40, 128, 166.5, 201.5, 251.8 nm with a constant solid perimeter (62%), C_{KCl}=0.4 d.)The local zeta potential average normalized with flat theory silica nanoparticle without designed particle solid perimeter value at D_p=40, 128, 166.5, 201.5, 251.8 nm **e.)** The solid, pore, local zeta potential average value normalized with flat theory silica nanoparticle at (pH=6).

Also, Figure 5.4 (a), (b), (c), (d), (e) parts are detailed to examine the effect of particle diameter changes according to the low ionic distribution environment. As mentioned above, the lower ionic concentration caused the development of thicker EDL on the surface of MSNs. Therefore, The physical effects of how to exposed to the mesoporous system were easily captured with results. Consequently, Figure 5.4 is focused on five different diameters of MSN that (Dp=40, 128, 166.5, 201.5, 251.8 nm) were designed at λ=15.8 nm where the ionic environment was C_{KCl}=0.4 mM. All MSN had

the same porosity (ϵ=0.42) and pore size values (H= 5 nm). Moreover, the solid perimeter (sp) of MSN kept constant the value of 0.62, lately. The 5.4.a. part of the figure explains to electric potential contour through a 45-degree area of the MSNs. The contours proved that the EDL effects were major on that system at lower ionic conditions where both pore inside and the entrance of the mesoporous system. The b. part of figure 5.4 demonstrate the undefined deviations of local zeta potential magnitude on the total mesoporous system. Therefore, the solid and pore average zeta potentials were calculated from along on the surface of MSNs for understanding which geometric case caused to the development of these extraordinary variations by taking into consideration predominant diverse physical effects. The c. part of figure 5.4 presents the average zeta potential magnitude both pore entrance and solid surface of silanol groups of MSNs. The c. part of the figure demonstrated that the $\zeta_{Solid\ ave}$ magnitude on the surface of MSNs obeyed the flat plate theory measurements. Moreover, the extraordinary electrokinetic potential behavior was discovered, and the particles were designed in taking consideration of solid perimeter constant before the constitution of the c part of figure 5.4. After the calculation of zeta potential magnitude, the figure demonstrated that the undefined variations of local ζ formed by geometric disorders of the mesoporous system. Hence d. and e. part of figure 5.4 display to answer how solid structure and pore entrance on the surface affect the local ζ_{ave} by the various particle diameter of MSNs. According to a result, when the particle diameter was lower than 150 nm, the physical effects such as curvature, EDL overlap developed on the solid structure, predominantly. Moreover, when the particle diameter was higher, the pore surface increased, as well. According to the e. part of figure 5.4, the decrease of local ζ_{ave} was observed because of the increase in the total number of pore entrance on the surface. However, when the small diameter of the solid particle was calculated, the 10% decrease was observed at D_p=40 nm. As a result, the various diameter of mesoporous silica nanoparticle system at high EDL thickness affected the local zeta potential magnitude. The physical effects were significant on both solid and pore zeta potential values. When the diameter of mesoporous silica nanoparticle is higher than 200 nm , the average magnitude of local zeta potantial approached to flat silica plate theory assumption. Therefore, the mesoporous behaviour at low ionic condition were predominant at lower diameter particle size.

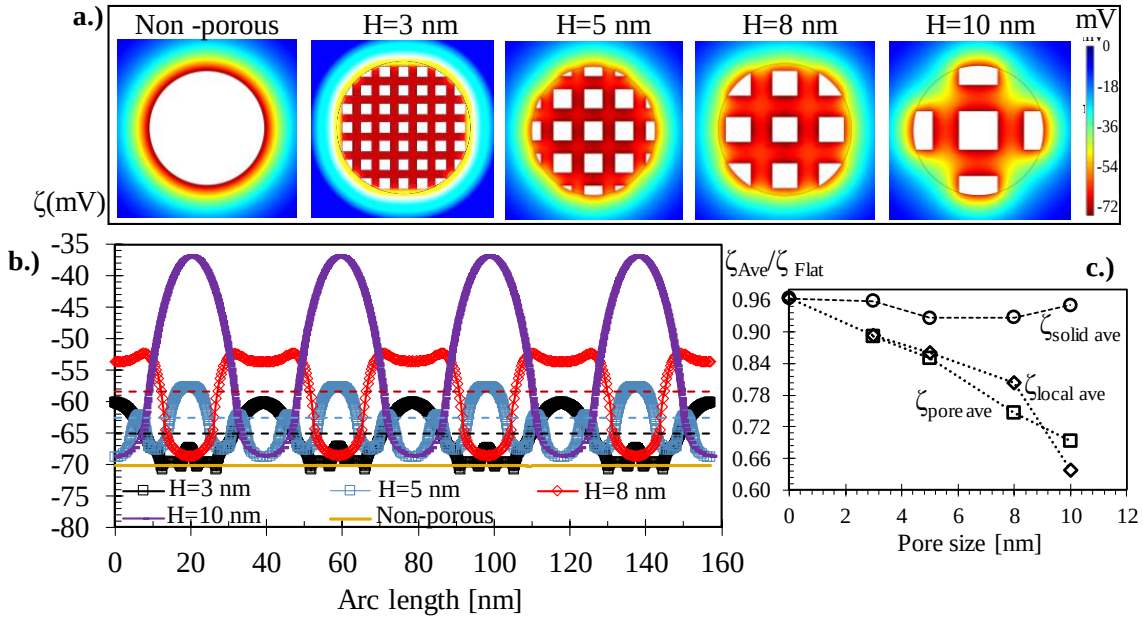

Figure 5.5. a.) The electrical potential response contours on the surface of MSNs. b.) Zeta potential distribution with varying H values at D_p=50 nm, ϵ=0.67, and C_{KCl}=0.4 mM. c.) The solid, pore, local zeta potential average value normalized with flat theory silica nanoparticle at C_{KCl}=0.4 mM (pH=6).

On the other hand, figure 5.5 (a-c) focuses on the small diameter of MSNs where are observed the local average zeta potential variations as properly. From a-c part fo figure 5.5. attempt to explain the behaviors of MSNs with different H values (3,5,8,10 nm) at constant ϵ=0.42, constant sp=0.44, C_{KCl}=0.4 mM, and $D_{particle}$=50 nm. Figure 5.5 (a-c) explains the creation of EDL overlap and curvature effect on high EDL thickness (λ) according to different H values. When the $D_{particle}$ was lower than 100 nm at high λ values, the physical effects were developed both inside and outside the mesoporous system, significantly. As seen that, the average magnitude of local zeta potential increased while the H values increased, as well. The predominant alteration of local ζ_{ave} according to H values were recognized in Figure 5.5. The small diameter of MSN had a lower surface to volume ratio so, the curvature effect created an inner side through pores. The pore inner interaction of silica nanoparticle represented a pore average zeta potential value. Therefore, the percentage of variations that both pore and local average demonstrated a similar trendline when the local and pore average zeta potential magnitude were normalized as a function of flat plate theory. However, the H=10 nm case, the percentage value of normalized $\zeta_{local\ Ave}$ magnitude decreased sharply due to the small solid surface area according to other cases. The decrease of pore number on the surface of MSNs caused the predominant of the $\zeta_{Pore\ Ave}$ on the mesoporous system. Therefore, the sharp

variation zeta potential values were observed between various H. As a result of that, the ionic distribution and the volume of pore structure of small MSNs were proportional to influenced more zeta potential deviations rather than larger MSN.

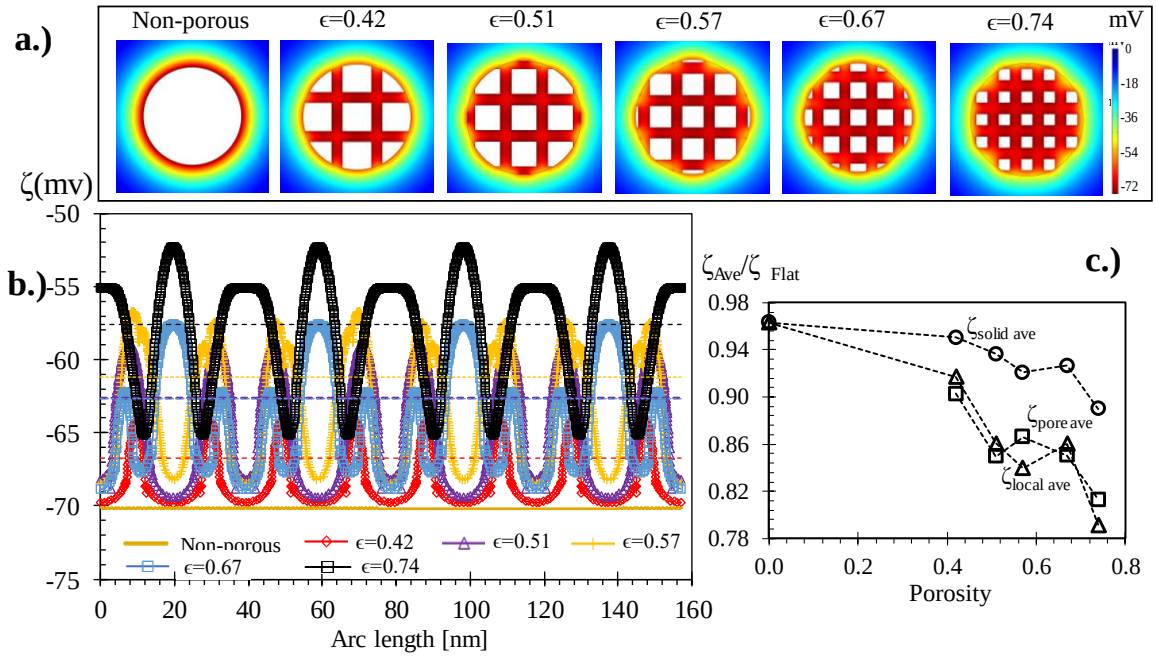

Figure 5.6. a.) The electrical potential response contours on the surface of MSNs. b.) Zeta potential distribution with varying ϵ values at D_p=50 nm, H=5 nm, and C_{KCl}=0.4 mM. c.) The solid, pore, local zeta potential average value normalized with flat theory silica nanoparticle at C_{KCl}=0.4 mM (pH=6).

Moreover, Figure 5.6 (a-c) point out that the magnitude ζave increases according to porosity raises. EDL overlap and curvature effect also were strongly active on MSNs at D_p=50 nm and CK_{Cl}=0.4 mM. The increases in pore numbers were obtained when the porosity increased. Therefore, strong pore corner effects were demonstrated on the high porosity values such as ϵ=0.57, 0.67, and 0.74. Furthermore, the ionic diffusion effect was seen sharply in both Figures 5.5 and 5.6. The changes of ζave value were observed at high porosity particle up to 40% according to flat plate theory measurement by analytical calculation. The electrokinetic difference of ions constituted surface charge regulation as a non-equivalent distribution into the pores. Moreover, the local, pore, size average zeta potential magnitude was normalized by flat plate theory. According to c.part of figure 5.6, the normalized pore average value showed the contrast behavior from solid and local normalized value. Because the corner effect observed more dominant at 0.57 porosity. This distribution led to revealing physical effects as a major essence at λ=15.8 nm both in Figure 5.5 and Figure 5.6.

$$\varepsilon_{3D} = \frac{N_{Pore}}{2} \times L_{Pore,Av} \times \frac{3}{2} \times \frac{D_{Pore}^2}{D_{Particle}^3} \tag{5.2}$$

$$\zeta_{MSNP} = \zeta_{Solid,Av} \times \left(1 - N_{Pore} \frac{D_{Pore}^2}{D_{Particle}^2} \right) + \zeta_{Pore,Av} \times N_{Pore} \frac{D_{Pore}^2}{D_{Particle}^2} \tag{5.1}$$

A number of pores were investigated to the calculation of local average zeta potential value in the three dimensional (3D) MSN system. Also, the solid and pore average zeta potential were measured by numerical analyses. The 3D measurement of pore size (D_{pore}) and diameter of particle ($D_{particle}$) was added to equation 5.1. The behavior of pore zeta potential average in the 3D environment (ζ_{MSNP}) was investigated by equation 5.1. The average zeta potential magnitude in the 3D system was estimated by using the D_{pore}, $N_{pore,}$ and area of total pores into the MSNs. Furthermore, the deviation of electrokinetic potential is sharply remarkable according to solid zeta potential average values at the small diameter of MSNs. Hence, the local zeta potential average of the 3D mesoporous system was demonstrated the deviation ratio according to the pore size-porosity/ MSNs diameter ratio. Moreover, the 3D porosity (ϵ_{3D}) was calculated by equation 5.2. The length of each pore was measured by COMSOL. The calculation of 3D porosity and local zeta potential value was correlated with each other for expressing the surface behaviors of MSNs when the physical effects were predominant in the 3D numerical measurement system. The main goal is to characterization of mesoporous silica nanoparticle by various 3-D particle size, porosity, and pore size. The number of pore size was found by cross section method on the different particle size of mesoporous silica nanoparticles. According to results, the average local zeta potential magnitude in 2-D environment was found same as with the 3-D average local zeta potential magnitude. Therefore, the 2-D cartesian system measurements showed real life results when the equation 5.1 and 5.2 were applied on the mesoporous silica nanoparticle system.

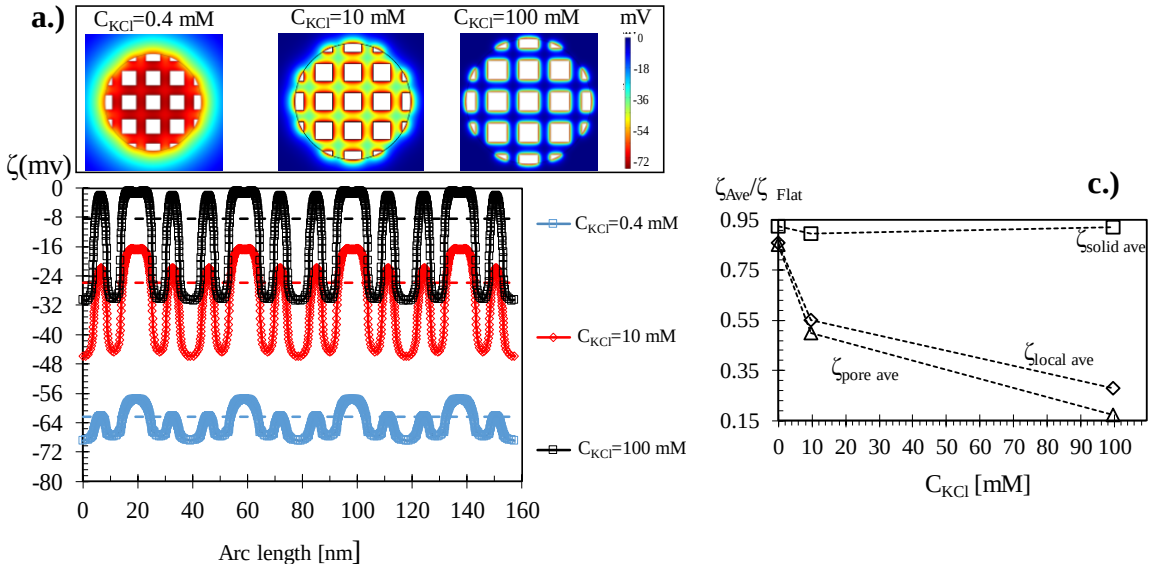

Figure 5.7. a.) The electrical potential response contours on the surface of MSNs. b.) Zeta potential distribution with varying ionic concentration values at D_p=50 nm, H=5 nm, and ϵ=0.67. c.) The solid, pore, local zeta potential average value normalized with flat theory silica nanoparticle at C_{KCl}=0.4, 10, 100 mM (pH=6).

Furthermore, figure 5.7 (a-c) demonstrates the discrete ionic environments on the MSN system. The physical effects were observed where the constant porosities of MSNs were ϵ=0.67, Dp=50 nm, and the various ionic molarity is C_{KCl} = 0.4, 10,100 mM. The lower ionic environment and small diameter of MSN caused the growth of EDL overlap, corner, and curvature effects at both pore inside and pore entrance. The average zeta potential magnitude increased when the ionic distribution was richest. Moreover, the curvature effect also developed on the solid structure when the higher EDL thickness (C_{KCl}=0.4 mM) Also, the corner effect led to the variation on the zeta potential magnitude at C_{KCl}=0.4 m where the solid/liquid interface was predominant. At C_{KCl}=100 mM case, the mesoporous system reaches the bulk concentration in the pore throat at a small diameter. The c part of figure 5.7 explains the normalized of average zeta potential magnitude as a function of the flat plate silica surface. The high ionic concentration showed sharp deviations according to pore and local average normalized value in contrast to a flat silica system. Moreover, each mesoporous system showed similar behavior with flat plate theory when the solid zeta potential average magnitude was considered by the c part of figure 5.7.

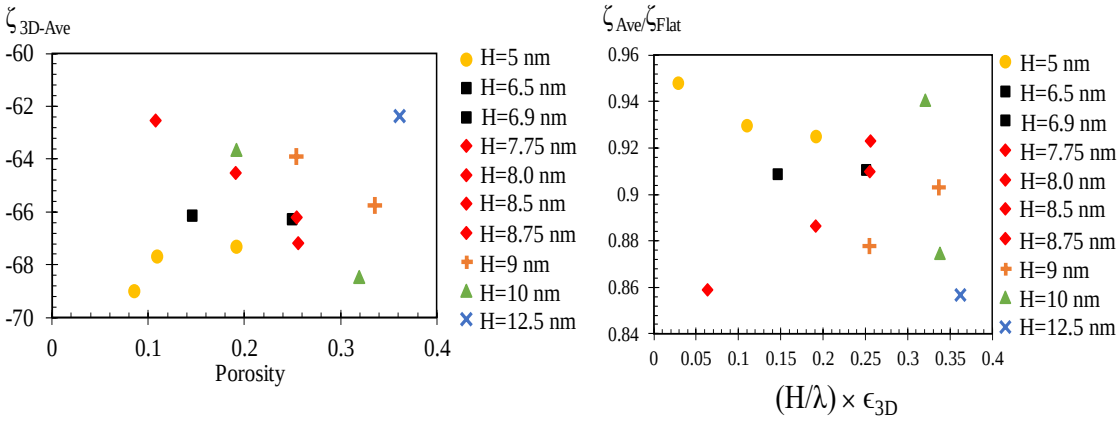

Figure 5.8. a.) Zeta potential distribution with H and ϵ_{3D} values at D_p=50 nm and C_{KCl} =0.4 mM. b.) Normalized local zeta potential value distribution for different H, ϵ_{3D}, diameters at constant C_{KCl}=0.4 mM for their variation according to the characterization of (H /λ) × ϵ_{3D}.

Figure 5.8 explains that the deviation zeta potential magnitude according to diverse ϵ and H values with high EDL thickness on the surface of the mesoporous system (λ=15.98 nm) at D_p=50 nm. The solid perimeter was kept constant (0.44) to all the various ϵ and H values for evaluating how the physical effects were showed variations when the numerical results were compared to flat plate theory. Therefore, the absolute zeta potential magnitude increased when the porosity decreased at the same H values. Also, the H values were the predominant key to demonstrate the variations of zeta potential magnitude with the surface of the small diameter of MSN. Moreover, ϵ_{3D} mostly affected the surface behavior on the surface of the porous silica nanosystem according to flat plate silica theory. The nondimensional parameter, which is (H /λ) × ϵ_{3D}, examined the behavior od mesoporous silica nanoparticle. The high ϵ and high H values created the EDL overlap at high EDL thickness value, corner and, curvature effect both pore entrance and pore throat on the MSNs so, the mesoporous system started not to obey the flat plate theory calculations. Moreover, the EDL thickness value was more than various pore size values in the mesoporous silica nanoparticle system. Therefore, the high pore size and porosity values demonstrated the physical effects on the zeta potential magnitude up to 10% according to flat plate theory calculations.

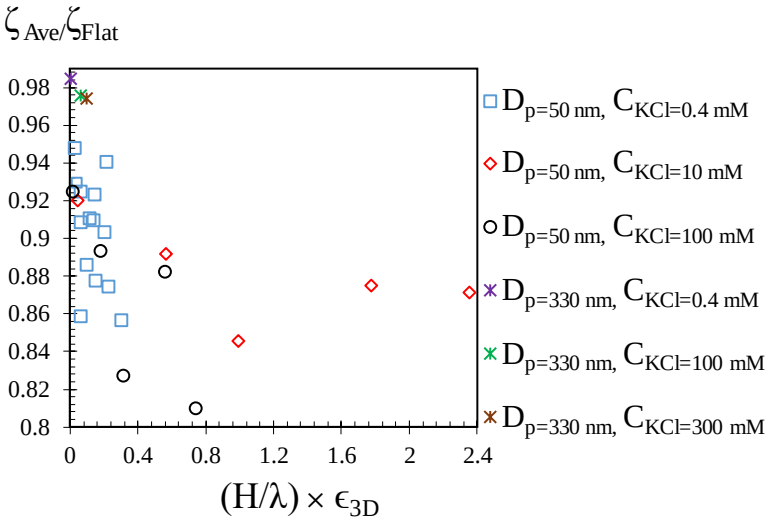

Figure 5.9. Normalized local zeta potential value distribution as a function of flat silica plate theory for different H, ϵ_{3D}, diameters(D_p=50,330nm), and ionic concentrations(C_{KCl}=0.4,10,100 mM) for their variation according to the characterization of (H /λ) × ϵ_{3D}.

In Figure 5.9, the analytical calculations are applied on small Dp with the various H and ϵ values and solid perimeter (0.44) according to different EDL thicknesses (λ=0.97 nm,3.08 nm, 15.98 nm). The local zeta potential average was normalized with the function of flat plate theory prediction. When the ζ_{ave} was calculated by used several ϵ values, although EDL overlap was observed either inside or outside the pores, the physical changes examined the predominant point for finding out major alterations on MSN systems. These physical changes illustrated how to be reached sharply to bulk concentration at higher EDL thickness regards to H and ϵ values. Moreover, the large diameter MSNs system reached the bulk system because, the physical effects were eliminated on the high diameter, low porosity.

5.2. Experimental Results:

In experimental results were evaluated to validate our multi-ion charge regulation model according to different salt ionic conditions, pH, surfactant effect, and various D_p. Aerosil90 (20 nm), Aerosil150 (16 nm), Aerosil200 (12 nm), OX50 (40 nm), and TT600 (40 nm) hydrophilic silica nanoparticles were bought from EVONIK company to do experiments. All experiment was figured by the utilization of every particle. All particles contained the amorphous SiO_2. However, most of the experiments were committed with

A200, A90, and OX50 particles due to their stabilization ratio according to high range solvent interaction with surface SiO_2 groups in the literature searching part. NaCl solid was used as a source of salt media. Furthermore, the SEM and STEM images were taken for proving our DLS method measurements.

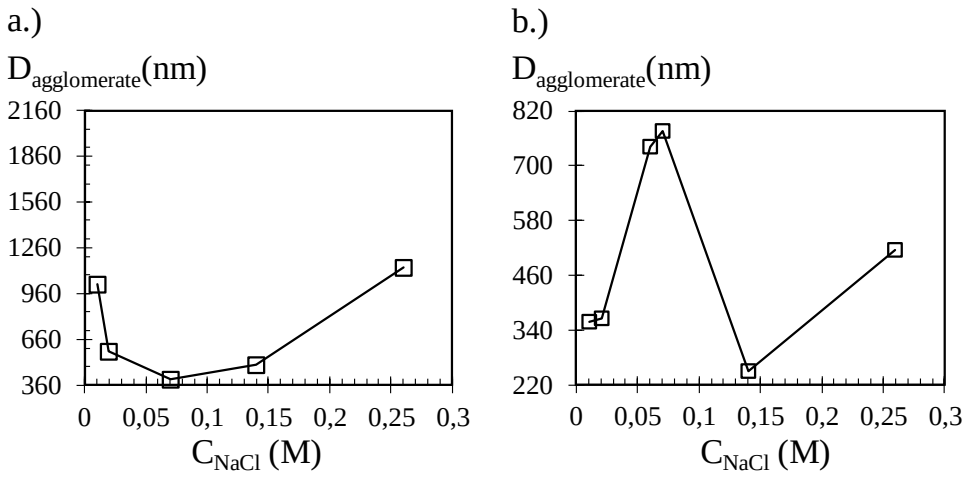

Figure 5.10. Precipitate quantities at different salt concentrations: **a.)** Precipitation nanoparticle diameter is demonstrated by the A200 (12 nm) particle to different salt concentration. **b.)** Precipitation nanoparticle diameter of the A90 (20nm) particle to the salt concentration of different valence.

In figure 5.10 demonstrates how monovalent cation (Na+) affects the solubility of silica into the DI water solvent for silica nanoparticle size measurements. According to previous studies discovered that silica nanoparticle dispersed in the DI water as the amount of 75-150 ppm. Therefore, the two different diameters of silica nanoparticle were prepared into the DI water solvent according to base on the literature knowledge. A200 (12 nm) and A90 (20 nm) silica particles were selected to experiment with the water solution sample. The polydispersity index was kept constant at 0.2 value. The pH of the two solutions was constant at 8 from taken 5.11 figure results. The $D_{agglomerate}$ results of each silica nanoparticles, which are A90 and A200, were compared with each other. Even though A200 and A90 particles have seemed like the same silica particle, the agglomeration ratio was different according to their hydrodynamic ratios. The hydrodynamic diameter ratio of A200 nanoparticle was lower than A90 nanoparticle concerning into the water solution. The lower hydrodynamic diameter ($D_{agglomerate}$ =400 nm) was observed at the lower salt concentration (C_{NaCl}=0.07 M) for A200 nanoparticle. However, the lower agglomeration diameter was found at 0.14 M NaCl solution,

$D_{agglomerate}$ =250.6 nm for A90 silica nanoparticle. The lower hydrodynamic diameter of amorphous silica nanoparticle was observed as a less agglomerate behavior for A90 silica nanoparticle. The tamped density of silica nanoparticle is the predominant factor for reaching the stabilization environment. The tamped density of A90 silica nanoparticle was 80 g/l, but the tamped density of A200 was 50 g/l. Therefore, the agglomeration ratio of A200 was observed higher value rather than A90 nanoparticle.

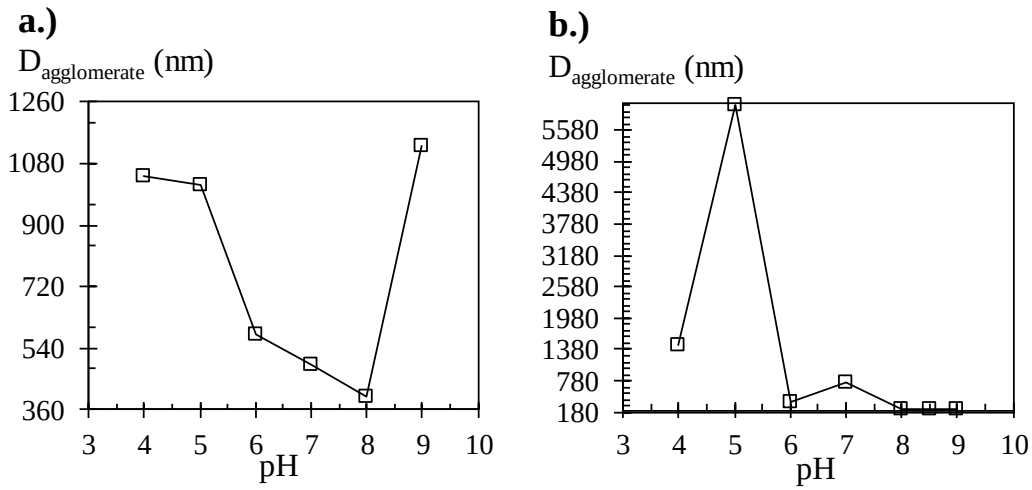

Figure 5.11. Precipitate quantities at different pH values: **a.)** Precipitation nanoparticle diameter is demonstrated by the A200 (12 nm) particle to the different pH value. **b.)** Precipitation nanoparticle diameter of the A90 (20nm) particle to the pH of different valence.

Also, In Figure 5.11, the silica solutions were prepared with various pH ionic conditions with added to their monovalent cation as the milligram amount into the water solution. For A200, the critical salt concentration was arranged with 0.07 M NaCl solution, whereas the critical salt concentration of A90 was selected the 0.14 M NaCl solution according to the results of figure 5.10. The polydispersity was kept constant at 0.2. In Figure 5.11, the a. part belongs to A200 silica nanoparticle and b. part belongs to A90 silica nanoparticle, the lowest diameter of silica nanoparticles were found at pH 8. However, the lowest diameter was found as a 392 nm for A200 and 246.2 nm for A90 silica nanoparticles. The association/dissociation reactions were predominant on both hydrophilic silica nanoparticles. According to results, the agglomerate diameter range was displayed for A200 nanoparticle for lower pH values. The tolerance of tending to stabilization of A90 nanoparticle was higher in an acidic environment than A200 silica nanoparticle. However, after pH=8, the behavior into the DI water demonstrated the difference between A90 and A200 silica nanoparticle. The highest agglomeration

behavior was observed for A200 at pH=9 value, but the agglomeration ratio was kept constant for A90 silica nanoparticle at pH=9. The importance of pH value was shown according to the investigation of the agglomerate ratio on the colloidal system.

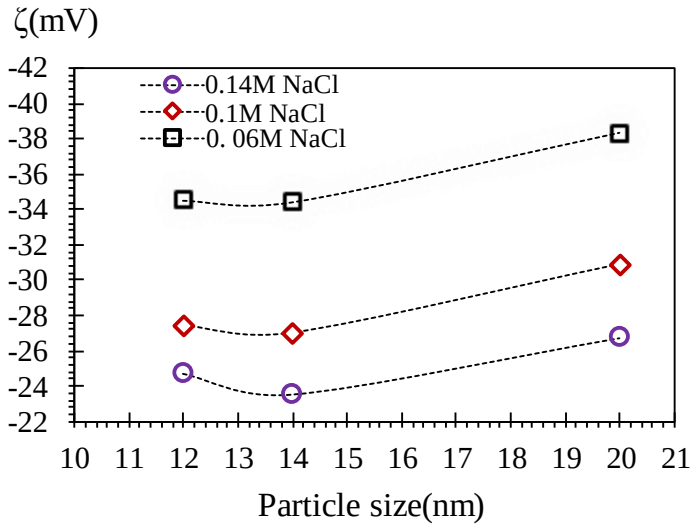

Figure 5.12. The experimental result of zeta potential distribution with particle size according to different salt concentrations.

In figure 5.12, the salt effect was investigated by the zeta potential magnitudes of each silica nanoparticle. The experimental studies about zeta potential measurement were done with A90 (20 nm), A150 (16 nm), and A200 (12 nm) by used a zeta sizer instrument. According to theoretical assumptions, EDL developed the opposite side of the particle on the surface, and the overlap occurs on the silica colloidal system in the lower salt ionic concentration environment. DI water was utilized as a solvent type. According to results, when the absolute average zeta potential magnitude decreases when the particle diameter increased at the same salt concentrations value. The absolute average zeta potential magnitude decreased according to lower salt concentration values. The average zeta potential magnitude behavior of experimental measurements was showed the same behavior according to our theoretical calculations.

According to the results of figure 5.13-14-15, the polymer dispersion, which was APA, was used to ensure of dissolving the silica nanoparticle regards to hydrodynamic ratio. In figure 5.13 shows the dispersion amount of silica into the APA surfactant. The agglomeration degree of silica nanoparticles could alter with various solutions that depended on the polar and non-polar ionic environment of the molecular bonding of chemicals. The nature of silica nanoparticle predominantly demonstrated the agglomerate form in the polar media. However, the polar side of the APA surfactant

reacted to the silanol groups (Si-OH) of the silica nanoparticle. Therefore, the repulsion force between the silica nanoparticle assisted to develop of the EDL (electric double layer) on the silica nanoparticles. Consequently, the agglomeration of the small silica nanoparticles was eliminated by the APA solvent. However, each solution had its solubility limits depend on the chemical bond interactions with Si-OH groups. Therefore, figure 5.13 displays the solubility rate of Aerosil 200 (12 nm) into the APA surfactant solvent as ppm (parts per million) range. The 1400 ppm (7mg) was the optimum solubility amount of the silica nanoparticle into the polyacrylate surfactant that the agglomeration was negligible even if small nanoparticles. APA surfactant decreased the steric hindrance to the colloidal system by using the electronegativity effect of the carboxylic functional group. Hence, the solubility rate was increased up to twenty times than the DI water solubility rate of the silica nanoparticle.

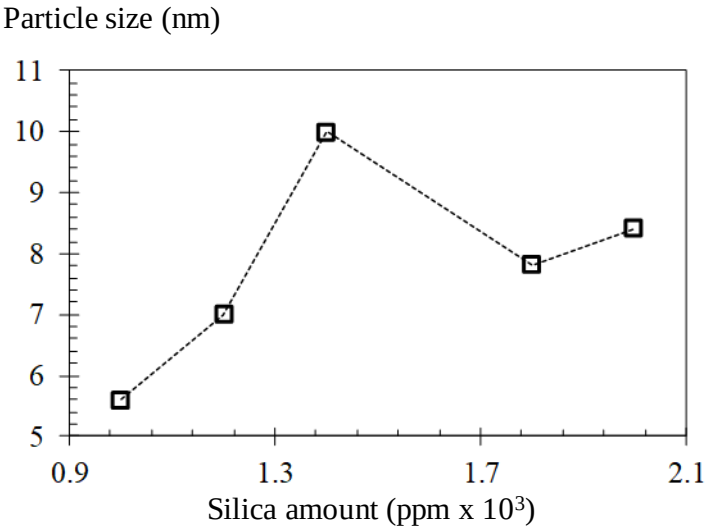

Figure 5.13. The effect of silica amount for experimental particle size measurement on the A200 (12 nm) particle.

Also, Figure 5.14 confirms to the effect of the APA volume ratio into the silica - surfactant solution. According to results, when the 4.0 ml of APA surfactant was utilized into the silica solution with 1 ml DI water, the accurate A200 silica nanoparticle size was measured 11.8 nm by DLS method. The dispersive volume of APA was found for A200 silica nanoparticle. Therefore, 7 mg of A200 silica nanoparticle amount and 4 ml APA surfactant amount was adjusted for other experimental size measurements. The ultrasonic process was applied for keeping distance between the nanoparticle according to their intermolecular force interactions. The steric repulsive force of anionic polymer dispersant of the APA molecule was mainly effective on amorphous silica nanoparticle

for avoiding the agglomeration of small silica nanoparticle. Because of the small size of nanoparticle eagers to being agglomerate rather than large silica nanoparticles. The pH was kept constant at 8 due to the control of the dispersion ratio of silica nanoparticle.

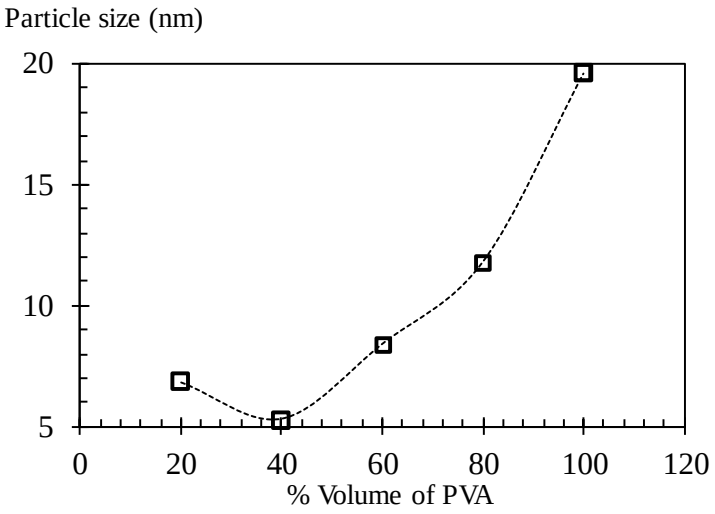

Figure 5.14. The effect of volume percentage of polymer dispersant (APA) for expr. particle size measurements on the A200 (12 nm) particle.

Furthermore, Figure 5.15 explains the pH effect on the particle size measurements. Protonation and deprotonation reactions had an impact on the surface of silica nanoparticle. Therefore, the results of figure 5.15 were showed to alteration of particle size according to pH value. According to figure 5.13-5.14 results, the 7 mg of silica nanoparticle immersed into 4 ml of APA surfactant. The ultrasonic process was applied for keeping distance between the nanoparticle according to their intermolecular force interactions. After pH 9, the silica nanoparticle started to swelling themselves so, the decrease of particle size observed in figure 5.15 at pH=9 value. Therefore, our experimental particle size measurement showed the same behavior at pH 8 value when the polymer dispersant of APA was used as a solvent. In acidic conditions, the dissolution of silica nanoparticles was predominant in the APA solution. Therefore, the unsaturation environment was observed according to results between pH 6-8.

Also, the decrease in size was considered after pH =8. According to results, the best pH environment was found for silica-APA dispersant solution at room temperature.

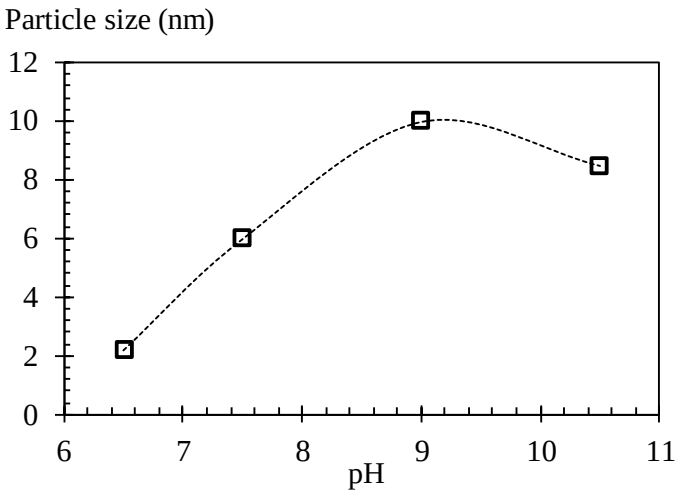

Figure 5.15. The effect of different pH values for experimental particle size measurements on the A200 (12 nm) particle

Also, figure 5.16 demonstrates the correlation between commercial particle size and experimental particle size measurements. Next, Figure 5.16 shows the variation of particle size measurements according to experimental results. As seen in figure 5.16, the accurate result was observed from Aerosil 90 (20 nm) and Aerosil 200 (12 nm) particles. APA absorbed the silanol groups of them as a competence. Moreover, the moiety percentage of silica nanoparticle was the key parameter to estimate the absorption ratio. According to figure 5.16, when the particle size increased, the absorption ratio of APA decreased. The repulsion force was activated by the size of EDL thicknesses. In small nanoparticles, the EDL thickness ratio was not negligible when it developed on the surface of silica nanoparticle as a layer.

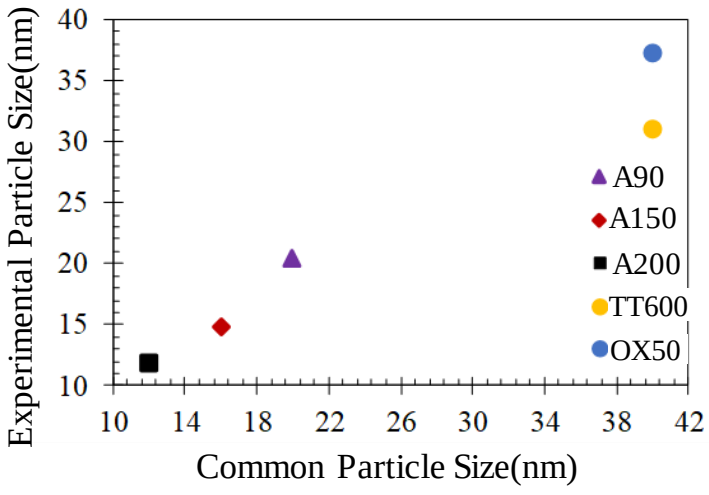

Figure 5.16. The comparison between the experimental measurements and literature measurements of A90, A150, A200, TT600 silica nanoparticles.

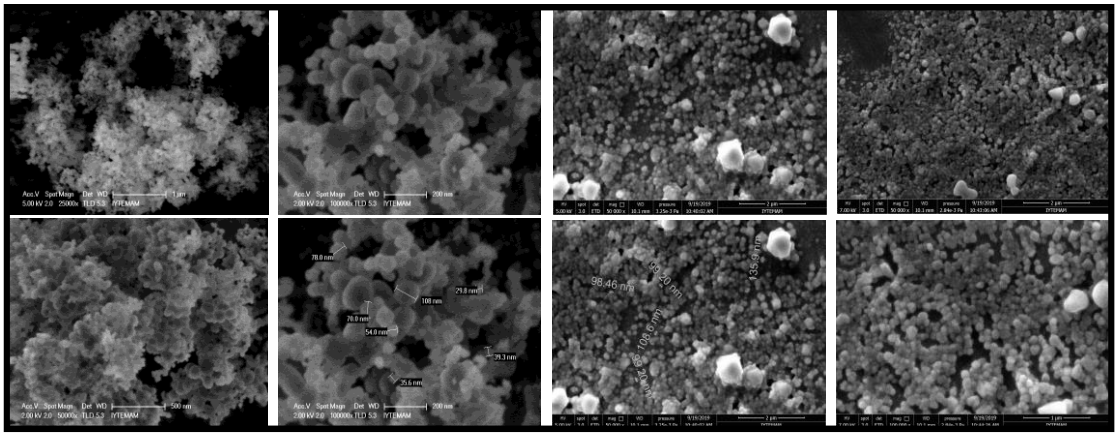

Figure 5.17. Scanning electron microscopy images of OX50 silica nanoparticle

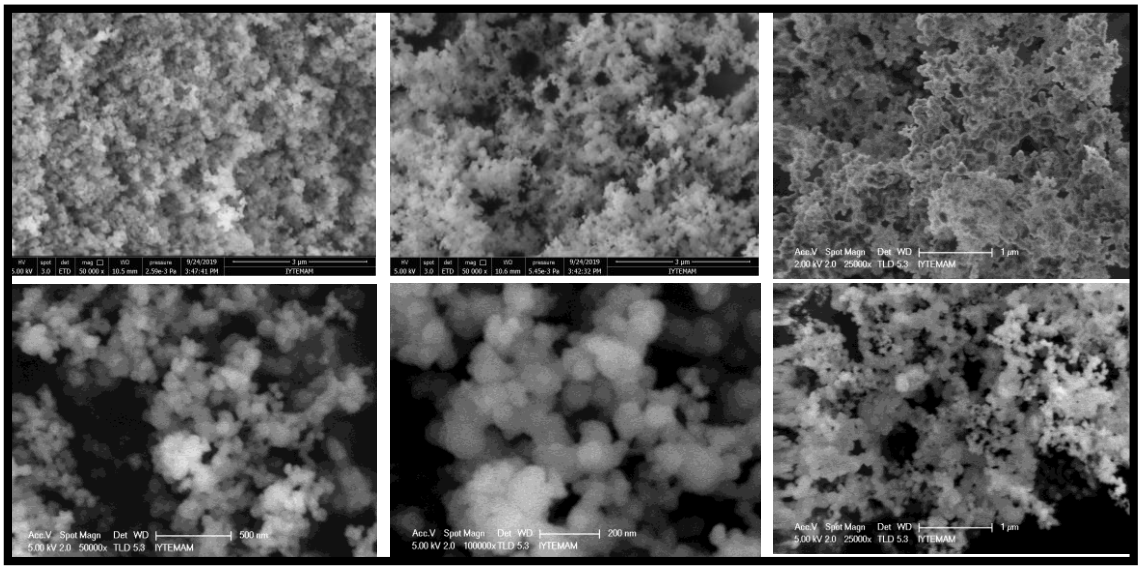

Figure 5.18. Scanning electron microscopy images of TT600 silica nanoparticles.

Figure 5.17-5.18-18-20 demonstrates the SEM and STEM images for A90, A200, OX50, and TT600. Each particle size was measured by the DLS method. After, STEM and SEM images procedures were applied to the particles to be scientifically proven of our DLS method. In figures displayed that means the particle size of each silica nanoparticle was found close to according to our DLS method measurements. However, the resolution of STEM and SEM were not permitted to capture of single-particle for each of the silica. Therefore, the STEM experiments were performed by utilization of the TEM grid for imaging the single silica nanoparticle between the grid layer. The 400 mesh carbon grids were immersed in the NaCl salt solution where is used by DI water. The pH is adjusted the 8 for colloidal stabilization. The second sample preparation was a dry powder method that the small number of powder samples, which were OX50 and TT600,

put on the carbon conductive tape. According to the preparation of sample solutions, which were dry and liquid silica samples, imaging results were taken by SEM instruments. The high and low kV were applied to the samples for catching a better resolution for imaging processes. The small silica nanoparticles tended to more agglomerate because of their lack of repulsive force between the nanoparticle. The electron backscattering detector was used to increases the sensitivity and resolution of SEM instruments. The results of SEM imaging displayed that the mean particle size of OX50, TT600, Aerosil 200, and Aerosil 90 nanoparticles were matched with DLS method measurements where the figure 5.16 demonstrates the experimental particle size results. Furthermore, the single silica nanoparticle was detected when the Aerosil 90 (20 nm) and Aerosil 200 (12 nm) was utilized by Tem Grid. However, the SEM imaging of Aerosil 150 silica nanoparticle was not shown clearly, because of the particle's moiety features. The same sample preparation was applied to the Aerosil 150 silica nanoparticle. However, the ratio of the moiety of own Aerosil 150 nanoparticle prevented to take clear imaging from SEM instruments. Therefore, the imaging of Aerosil 150 was not caught properly.

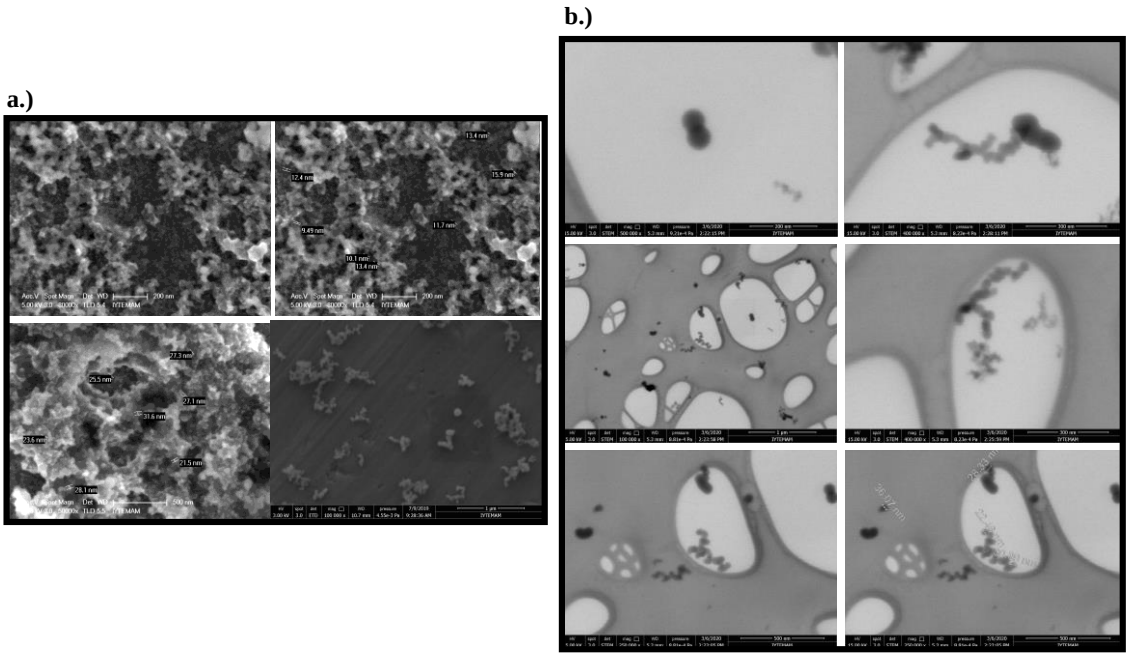

Figure 5.19. Scanning electron microscopy images **a.)**SEM, **b.)**STEM of Aerosil90 silica nanoparticle.

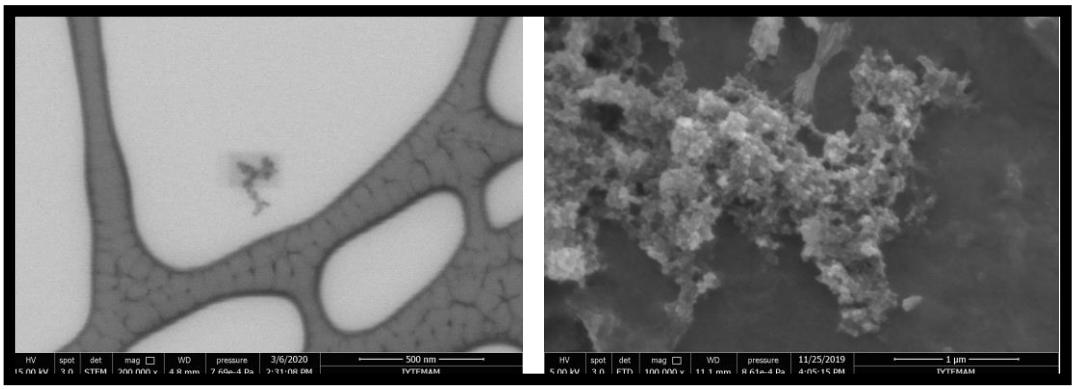

Figure 5.20. Scanning electron microscopy images of Aerosil200 silica nanoparticle.

In figure 5.21 (a-b) part displays the FTIR results of all silica particles which are A90, A150, A200, OX50, and TT600. In figure 5.21 a.) and b.) demonstrates that the FTIR peak provides to explain the surface modification of silica nanoparticle when APA polymer dispersant was used as a solvent. The sharp absorbance peak at 1700 cm $^{-1}$ explains the bond power between silica and amide group interact by resonance form of the polar-polar intermolecular force. Broad peaks, where appeared between 1700 and 1400 cm $^{-1}$, provided to express the bending vibrational bond of the C-H in the acrylic copolymer. Moreover, the reasons for emerging to vibrational bond at 3400 cm $^{-1}$ were defined with two constituents: the stretching bond raised by the H-O bond where came from moisturizing at that wavelength or the absorbance peak of silica particle that was not be encapsulated by acrylic copolymer. On the other hand, the significant peak of figure 5.21 shows at 1150 cm $^{-1}$ where the Si-O-Si bending bond occurs, spontaneously. The bond appeared between 2900 and 3200 cm^{-1} clued that methyl and ethyl group introduce their absorbance peak with the acrylic copolymer.

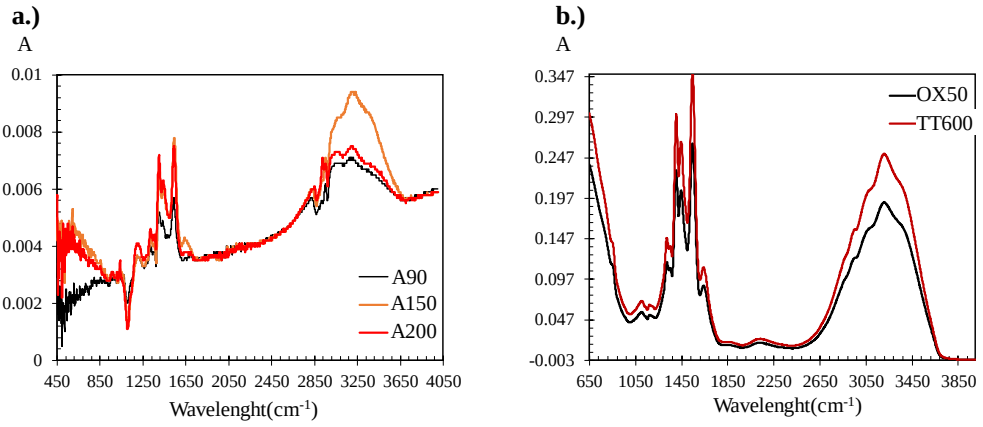

Figure 5.21. FTIR results of **a.)** Aerosil90, 150, 200 nonporous silica nanoparticle, **b.)** OX50, TT600 nonporous silica nanoparticles.

Furthermore, table 5.1 is demonstrated to experimental results for each silica nonporous particle. The surface area of each silica nanoparticle was measured by the BET experiment. The BET results of OX50, TT600, Aerosil90, Aerosil150, and Aerosil 200 were 46.5764, 80.7589, 86.7289, 140.9173, and 183.3941 m^2/g. According to BET results, the surface area increased where the particle size decreases in experimental analyses.

Table 5.1. Experimental BET values at 25°C for diverse silica nanoparticles.

Aerosil Silica Particle	Literature P.S (nm)	Literature BET (m^2/g)	Experimental P.S. Results (nm)	Experimental BET Results (m^2/g)
OX50	40	35-65	37.1	46.5764
TT600	40	150-250	31	80.7589
A90	20	75-105	20.4	86.7289
A150	16	135-165	14.8	140.9173
A200	12	175-225	11.8	183.3941

CHAPTER 6

SUMMARY AND CONCLUSION

Mesoporous silica nanoparticles (MSNs) are the new nanoparticle class with pore sizes between 3-20 nm and the particle diameters between 30-500 nm. The types of MSN are classified by their various pore shapes and synthesis procedures. Following the discovery of MSN, both natural science and engineering areas utilized them in applications, such as electrokinetic devices, sensors, and biomedical devices. MSNs are the excellent tunable materials with their highly ordered surface to volume ratio, pore size, low toxicology, and thermodynamic stability. Moreover, MSNs are good biodegradable material in targeted drug delivery. The surface charge of the mesoporous silica nanoparticle is the critical factor to design the targeted drug delivery mechanism. The protonation and deprotonation reactions determine the surface charge distribution on the mesoporous silica nanoparticle. However, the existing literature only explains the surface charge by Boltzmann distribution. However, Boltzmann distribution only valid certain conditions: zeta potential of MSNs must be lower than 25 mV; the surface of MSNs must be flat and sufficiently away from any other bodies. Therefore, the Poisson Boltzmann (PB) equation is suitable to measure electrokinetic potential calculations on the flat silica system. When the EDL overlap, curvature effect, and corner effect are developed in the MSNs system, the PB equation is not appropriate to solve the correct local zeta potential value on the silica particle's surface. Therefore, Poisson -Nernst- Plank (PNP) equation is applied to the mesoporous silica system to calculate the mesoporous system's surface charges. Also, the local zeta potential demonstrates variations on the silica particle's surface, the Charge Regulation model is used as a boundary condition and solved with the PNP equation.

This study aims to characterize both large and small particle sizes of MSNs with various pore size, porosity, and ionic concentration parameters by numerical modeling measurements. The Poisson-Nernst-Planck equation is solved by the Charge Regulation model. When the EDL overlap is developed on the surface of a mesoporous silica nanoparticle in the low ionic environment, the local zeta potential magnitude shows variations. The deviations cause to change the equilibrium of the nanosystem. Therefore,

the behavior of MSNs is unpredictable. Another physical effect, which is the curvature effect, creates the zeta potential value deviation when the surface to volume ratio is decreased. Also, the corner effect is observed on the mesoporous system's pore throat due to the overlap of EDLs. The zeta potential characterization of MSNs is defined according to these physical effects. Therefore, MSNs were designed for the investigation into how geometrical properties affected on the zeta potential magnitude when the physical effects developed on the mesoporous system.

Firstly, different pore size, porosity, and ionic concentration were studied at a large diameter of MSNs (Dp =330 nm). The solid perimeter was kept constant for each nanoparticle to eliminate the geometric disorder. The average absolute zeta potential magnitude decreased when the pore size increased on large diameter MSNs. The EDL overlap effect was not demonstrated on the surface of the large-diameter MSNs. Because the EDL thickness was less than pore size value. However, the EDL overlap was observed in the pores at the lowest pore size value. The zeta potential magnitude of solid parts obeyed the PB flat surface theory potential measurements. Also, the curvature effect was not predominant on the large diameter, pore size, and low porosity particle. Secondly, the various porosities were designed at the large diameter of mesoporous silica nanoparticles at low EDL thicknesses. The results showed that the absolute magnitude of zeta potential increased, when the porosity increased, as well. In the highest porosity case, the EDL overlap occurred to the opposite side of the pore, so the variation on the average absolute zeta potential was observed at a high porosity case. The solid part of the zeta potential showed the same behavior with flat surface theory estimation. Moreover, the corner effect was observed at the pore throat with high porosity values due to the increase of the pore number. The corner effect and EDL thickness caused to zeta potential variations on the mesoporous system. In the next step, the various ionic salt conditions were simulated at low porosity and large diameter MSNs. The average absolute zeta potential value decreased by the decrease of concentrations. The predominant factor of these variations was EDL overlap effects on the mesoporous system at low salt concentration. Also, the corner effect created lower ionic distribution on the surface of the nanoparticle. However, there was no significant curvature effect was observed both low and high ionic concentrations at large diameter. Therefore, the variation of zeta potential value cannot be predicted with flat theory assumptions. Next, the curvature effect was investigated at different diameters with constant porosity, pore size, and solid perimeter. The EDL overlap has been seen in both large and small diameters of MSNs. However, the curvature

effect was significant where the particle size decreased. Therefore, the average absolute zeta potential magnitude of each mesoporous particle was found far away from flat surface behavior. The zeta potential of large diameter mesoporous systems was found to be defined according to geometric properties such as porosity, pore size. The ionic distribution and these geometric properties were found to determine the zeta potential. Also, the predominant physical effects are evaluated at a large diameter mesoporous system.

According to the above information, the various pore size, porosity, and ionic concentration were studied at a small diameter of MSNs. Results defined that the average absolute zeta potential magnitude showed the same behavior for both large and small diameter of MSNs by various pore size, porosity, and ionic concentration. However, the physical effects were caused to demonstrate significant variations on the local, pore, and solid zeta potentials. The local average zeta potential value variations displayed the same behavior with pore average zeta potential value. Therefore, the EDL overlap in the pores is a critical factor for characterizing the MSNs at a small diameter. The equation was created to characterize the universal behaviors of three-dimensional zeta potential magnitude at each diameter of the porous system. Last, the 3-D local average absolute zeta potential magnitude was normalized by the flat plate theory with the various pore size, porosity, diameter, and ionic concentration. The normalized values were categorized by the nondimensional group ((ε3D×(DPore/λ)). The investigation of physical effects is examined specifically for the mesoporous system. The characterization of the mesoporous system was defined by the nondimensional group. Therefore, the requirement of the utilization of new modeling, which is multi-ion active charge regulation modeling, was understood for the mesoporous system.

Also, the stability and dispersion of nanoparticle are the critical factors in colloidal studies for targeted drug delivery mechanisms. The hydrophilic behavior of silica nanoparticle makes them easily agglomerate in water solvents. The agglomeration of silica nanoparticle is observed by particle size measurements. The new sample preparation steps have been developed by scientists for the elimination of this issue. According to studies, the number of monovalent cations affects the EDL thickness on the surface of the colloidal system. The protonation/deprotonation reaction is controlled by the alteration of pH value. pH is the critical factor to understand the stability of colloidal nanoparticles. The pH value affects the H+ donor/acceptor mechanism. This mechanism determines the surface charge density of the nanosystem. Therefore, the pH value directly

relates to the agglomerate ratio of silica nanoparticle. Also, the polymeric dispersion is utilized for a silica solution to increase stability. The polymer dispersion allows modification on the surface of silica nanoparticle. This surface modification impresses the surface charge density of the colloidal system. The dispersion degree of silica powder increases into the polymeric dispersion. According to this information, the experimental studies were done with diverse salt concentrations, pH, the volume of polymer dispersions, and critical salt amount. The DLS (direct light scattering) method was utilized for the particle size measurements. The optimum conditions were found according to other experimental studies from the literature. The best pH, silica amount, and polymer dispersion volume have been investigated through particle size measurements. According to particle size measurements, the dispersion of silica was succeeded in polymeric dispersion solution. After that, the zeta potential measurements were done at diverse salt concentration solutions. The results showed that the absolute magnitude of average zeta potential increased, when the particle size increased, as well. Also, the average absolute zeta potential decreased when salt concentration increased. The results showed that our numerical calculations are validated by experimental studies. Last, the sample was prepared to take the image of various silica nanoparticle using a Scanning Electron Microscope. Dry and liquid samples were prepared. For small silica nanoparticle, TEM Grid was used to capture a single nanoparticle on the SEM analysis.

REFERENCES

Jaroniec, M. et al., (2009), Silicon beyond the valley, p. 166.

Exley, C. et al., (1998),Silicon in life: A bioinorganic solution to bioorganic essentiality, p. 139-144.

Jugdaohsingh, R., et al.,(2002), Dietary silicon intake and absorption,p. 887-93.

Li, Z., et al.,(2012), Mesoporous silica nanoparticles in biomedical applications,p. 2590-605.

Slowing, I.I., et al., (2010), Mesoporous silica nanoparticles: structural design and applications. p.37.

Lee, C.H., et al., (2009), Near-Infrared Mesoporous Silica Nanoparticles for Optical Imaging: Characterization and In Vivo Biodistribution, p. 215-222.

Tarn, D., et al., (2013), Mesoporous silica nanoparticle nanocarriers: biofunctionality and biocompatibility. p. 792-801.

Chen, Y., H. Chen, and J. Shi et. al., (2013), In vivo bio-safety evaluations and diagnostic/therapeutic applications of chemically designed mesoporous silica nanoparticles, p. 3144-76.

Freitas, L.B.d.O., et al., (2017), Multifunctional mesoporous silica nanoparticles for cancer-targeted, controlled drug delivery and imaging, p. 271-283.

Lu, J., et al., (2010),Biocompatibility, biodistribution, and drug-delivery efficiency of mesoporous silica nanoparticles for cancer therapy in animals, p. 1794-805.

Chen, J.-F., et al., (2004), Preparation and characterization of porous hollow silica nanoparticles for drug delivery application, p. 723-727.

Kwon, S., et al., Silica-based mesoporous nanoparticles for controlled drug delivery, p. 2041731413503357.

Ströber W., et al., (1968), Controlled growth of monodisperse silica spheres in the micron size range, p.62-69

Kresge C.T., et al., (1992),Ordered mesoporous molecular sieves synthesized by a liquid-crystal template mechanism, p.710-712.

Na, H.K., et al., (2012), Efficient Functional Delivery of siRNA using Mesoporous Silica Nanoparticles with Ultralarge Pores, p. 1752-1761.

Foglia, M.L., et al., (2011), Recent patents on the synthesis and application of silica nanoparticles for drug delivery, p. 54-61.

Corriu, R.J.P. and D. Leclercq, (1996), Recent developments of molecular chemistry for sol-gel processes, p. 1420-1436.

Xie, J., S. Lee, and X. Chen, (2010), Nanoparticle-based theranostic agents, p. 1064-79.

Bharti, C., et al., (2015), Mesoporous silica nanoparticles in target drug delivery system: A review, p. 124-33.

Luis, Jean, (2009), Surface functionalized mesoporous silica nanoparticles for intracellular drug delivery, p. 31-47

Selvam, P., S.K. Bhatia, and C.G. Sonwane, (2001), Recent advances in processing and characterization of periodic mesoporous MCM-41 silicate molecular sieves, p. 3237-3261.

Gary-Bobo, M., et al., (2012), Cancer therapy improvement with mesoporous silica nanoparticles combining targeting, drug delivery and PDT., p. 509-515.

Yeh, Y.-Q., C.-Y. Tang, and C.-Y. Mou, (2014), Two-dimensional crystals of mesoporous silica SBA-15 nanosheets with perpendicular and open channels, p.72-83.

Tuysuz, H., et al., (2008), Direct imaging of surface topology and pore system of ordered mesoporous silica (MCM-41, SBA-15, and KIT-6) and nanocast metal oxides by high resolution scanning electron microscopy, p. 11510-7.

Albanese, A., P.S. Tang, and W.C. Chan, (2012), The effect of nanoparticle size, shape, and surface chemistry on biological systems., p. 1-16.

Ashley, C.E., et al., (2011), The targeted delivery of multicomponent cargos to cancer cells by nanoporous particle-supported lipid bilayers, p. 389-97.

Nel, A.E., et al., (2009), Understanding biophysicochemical interactions at the nano-bio interface, p. 543-557.

Gratton, S.E., et al., (2008), The effect of particle design on cellular internalization pathways, p. 11613-8.

Bobo, D., et al., (2016), Nanoparticle-Based Medicines: A Review of FDA-Approved Materials and Clinical Trials to Date, p. 2373-87.

Heikkila, T., et al., (2010), Cytotoxicity study of ordered mesoporous silica MCM-41 and SBA-15 microparticles on Caco-2 cells, p. 483-94.

Hecht, F., et al., (2016), The role of oxidative stress on breast cancer development and therapy, p. 4281-91.

Freeman, E.C., L.M. Weiland, and W.S. Meng, (2013), Modeling the proton sponge hypothesis: examining proton sponge effectiveness for enhancing intracellular gene delivery through multiscale modeling, p. 398-416.

Finlay, J., et al., (2015), Mesoporous silica nanoparticle delivery of chemically modified siRNA against TWIST1 leads to reduced tumor burden, p. 1657-66.

Wilhelm, S., et al., (2016), Analysis of nanoparticle delivery to tumours, p.751-760.

Hoshyar, N., et al., (2016), The effect of nanoparticle size on in vivo pharmacokinetics and cellular interaction, p. 673-92.

Fang, J., H. Nakamura, and H. Maeda, (2011), The EPR effect: Unique features of tumor blood vessels for drug delivery, factors involved, and limitations and augmentation of the effect, p. 136-51.

Siefker, J., P. Karande, and M.O. Coppens, (2014), Packaging biological cargoes in mesoporous materials: opportunities for drug delivery, p. 1781-93.

Yu, T., et al., (2012), Influence of geometry, porosity, and surface characteristics of silica nanoparticles on acute toxicity: their vasculature effect and tolerance threshold, p. 2289-301.

Kay, J.G. and S. Grinstein, (2011), Sensing phosphatidylserine in cellular membranes, p. 1744-55.

Dogra, P., et al., (2018), Establishing the effects of mesoporous silica nanoparticle properties on in vivo disposition using imaging-based pharmacokinetics, p.1154-1168.

Mei, L., et al., (2016), Electrophoresis of pH-regulated nanoparticles: impact of the Stern layer, p. 9927-34.

Das, P.K., (2016), Effect of thermodiffusion on pH-regulated surface charge properties of nanoparticle, p. 347-55.

Fogolari, F., A. Brigo, and H. Molinari, (2002), The Poisson-Boltzmann equation for biomolecular electrostatics: a tool for structural biology, p. 377-92.

Grochowski, P. and J. Trylska, (2008), Continuum molecular electrostatics, salt effects, and counterion binding--a review of the Poisson-Boltzmann theory and its modifications, p. 93-113.

Yeh, L.-H., et al., (2012), Field Effect Control of Surface Charge Property and Electroosmotic Flow in Nanofluidics, p. 4209-4216.

Namjesnik, D., et al., (2016), Application of the surface potential data to elucidate interfacial equilibrium at ceria/aqueous electrolyte interface, p. 825-837.

Abendroth, R.P., (1972), Surface charge development of porous silica in aqueous solution, p. 2547-2549.

Salis, A., et al., (2010), Ion specific surface charge density of SBA-15 mesoporous silica, p. 2484-90.

Shi, Y.-R., et al., (2018), Experimental Determination of Particle Size-Dependent Surface Charge Density for Silica Nanospheres, p. 23764-23771.

Kobayashi, M., et al., (2005), Aggregation and charging of colloidal silica particles: effect of particle size, p. 5761-9.

Atalay, S., et al., (2014), Surface Charge of a Nanoparticle Interacting with a Flat Substrate, p. 10927-10935.

Jiang, Z. and D. Stein, (2011), Charge regulation in nanopore ionic field-effect transistors, p. 031203.

Ninham, B.W. and V.A. Parsegian, (1971), Electrostatic potential between surfaces bearing ionizable groups in ionic equilibrium with physiologic saline solution, p. 405-428.

Barisik, M., et al., (2014), Size Dependent Surface Charge Properties of Silica Nanoparticles, p. 1836-1842.

Brown, M.A., et al., (2016), Determination of Surface Potential and Electrical Double-Layer Structure at the Aqueous Electrolyte-Nanoparticle Interface, p.2157-2188.

Inagaki, S., Y. Fukushima, and K. Kuroda,(1993), Synthesis of highly ordered mesoporous materials from a layered polysilicate, p.128-163.

Beck, J.S., et al., (1992), A new family of mesoporous molecular sieves prepared with liquid crystal templates, p. 10834-10843.

Trewyn, B.G., et al., (2007), Synthesis and functionalization of a mesoporous silica nanoparticle based on the sol-gel process and applications in controlled release, p. 846-53.

Zhao, D., et al., (1998), Triblock copolymer syntheses of mesoporous silica with periodic 50 to 300 angstrom pores, p. 548-52.

Zhao, D., et al., (1998), Nonionic Triblock and Star Diblock Copolymer and Oligomeric Surfactant Syntheses of Highly Ordered, Hydrothermally Stable, Mesoporous Silica Structures, p. 6024-6036.

Kim, T.-W., et al., (2004), Tailoring the Pore Structure of SBA-16 Silica Molecular Sieve through the Use of Copolymer Blends and Control of Synthesis Temperature and Time, p. 11480-11489.

Chen, Z., et al., (2015), Synthesis and drug delivery of mesoporous silica nanoparticles for cancer therapy, p.30-36.

Vallet-Regi, M., et al., (2001), A New Property of MCM-41: Drug Delivery System, p. 308-311.

Slowing, II, et al., (2009), Mesoporous silica nanoparticles for reducing hemolytic activity towards mammalian red blood cells, p. 57-62.

Wang, X., et al., (2014), Targeted delivery of tumor suppressor microRNA-1 by transferrin-conjugated lipopolyplex nanoparticles to patient-derived glioblastoma stem cells, p. 839-46.

Yu, B., et al., (2014), Insight into Mechanisms of Cellular Uptake of Lipid Nanoparticles and Intracellular Release of Small RNA, p. 2685-2695.

Townson, J.L., et al., (2013), Re-examining the size/charge paradigm: differing in vivo characteristics of size- and charge-matched mesoporous silica nanoparticles, p. 16030-3.

Kankala, R.K., et al., (2020), Nanoarchitectured Structure and Surface Biofunctionality of Mesoporous Silica Nanoparticles, p. e1907035.

Kim, H.L., et al., (2014), Enhanced tumor targetability of PEGylated mesoporous silica nanoparticles on in vivo optical imaging according to their size, p. 31318-31322.

Gan, Q., et al., (2012), Effect of size on the cellular endocytosis and controlled release of mesoporous silica nanoparticles for intracellular delivery, p. 259-70.

Forest, V., M. Cottier, and J. Pourchez, (2015), Electrostatic interactions favor the binding of positive nanoparticles on cells: A reductive theory, p. 677-680.

Nam, L., et al., (2018), Drug Delivery Nanosystems for the Localized Treatment of Glioblastoma Multiforme, p.525-542.

Muhamad, N., T. Plengsuriyakarn, and K. Na-Bangchang, (2018), Application of active targeting nanoparticle delivery system for chemotherapeutic drugs and traditional/herbal medicines in cancer therapy: a systematic review, p. 3921-3935.

Liu, H.J. and P. Xu, (2019), Smart Mesoporous Silica Nanoparticles for Protein Delivery, p.563-577.

Florek, J., R. Caillard, and F. Kleitz, (2017), Evaluation of mesoporous silica nanoparticles for oral drug delivery - current status and perspective of MSNs drug carriers, p. 15252-15277.

Duncan, R., (2003), The dawning era of polymer therapeutics, p. 347-60.

Sen, T. and M. Barisik, (2019), Internal surface electric charge characterization of mesoporous silica, p. 137.

Xu, C., et al., (2015), Core-Cone Structured Monodispersed Mesoporous Silica Nanoparticles with Ultra-large Cavity for Protein Delivery, p. 5949-55.

Shin, H.S., Y.K. Hwang, and S. Huh, (2014), Facile Preparation of Ultra-Large Pore Mesoporous Silica Nanoparticles and Their Application to the Encapsulation of Large Guest Molecules, p. 1740-1746.

Zhu, X., et al., (2019), Non-spherical micro- and nanoparticles in nanomedicine, p. 1094-1121.

Sun, J., et al., (2006), Ultrafast enzyme immobilization over large-pore nanoscale mesoporous silica particles, p. 1322-4.

Hartmann, M., (2005), Ordered mesoporous materials for bioadsorption and biocatalysis, p. 4577-4593.

Knezevic, N.Z. and J.O. Durand, (2015), Large pore mesoporous silica nanomaterials for application in delivery of biomolecules, p. 2199-209.

Yu, T., A. Malugin, and H. Ghandehari, (2011), Impact of silica nanoparticle design on cellular toxicity and hemolytic activity, p. 5717-28.

Zhang, J.X., et al., (2012), Magnetic mesoporous silica nanospheres as DNA/drug carrier, p. 379-382.

Huang, J., et al., (2009), Influence of pH on the stability characteristics of nanofluids, p. 879-+.

Zhao, H., X. Kang, and L. Liu, (2005), Comb−Coil Polymer Brushes on the Surface of Silica Nanoparticles, p. 10619-10622.

Jiang, L., L. Gao, and J. Sun, (2003), Production of aqueous colloidal dispersions of carbon nanotubes, p. 89-94.

Lee, K., et al.,(2009), Performance evaluation of nano-lubricants of fullerene nanoparticles in refrigeration mineral oil, p. E128-E131.

Li, X.F., et al., (2008), Thermal conductivity enhancement dependent pH and chemical surfactant for Cu-H2O nanofluids. Thermochimica Acta, 2008. **469**(1-2): p. 98-103.

Assael, M.J., et al., (2005), Thermal conductivity enhancement in aqueous suspensions of carbon multi-walled and double-walled nanotubes in the presence of two different dispersants, p. 647-664.

Shahrul, I.M., et al., (2016), Experimental investigation on Al2O3–W, SiO2–W and ZnO–W nanofluids and their application in a shell and tube heat exchanger, p. 547-558.

Li, Z.F., et al., (1998), Covalent immobilization of glucose oxidase on the surface of polyaniline films graft copolymerized with acrylic acid, p. 45-53.

Franchina, J.G., et al., (1999), Electrostatic immobilization of glucose oxidase in a weak acid, polyelectrolyte hyperbranched ultrathin film on gold: fabrication, characterization, and enzymatic activity, p. 3133-9.

Alan, B.O., M. Barisik, and H.G. Ozcelik, (2020), Roughness Effects on the Surface Charge Properties of Silica Nanoparticles, p. 7274-7286.

Bianchi, E., et al., (2017), Inverse patchy colloids: Synthesis, modeling and self-organization, p. 8-15.

Stroock, A.D. and G.M. Whitesides, *Controlling flows in microchannels with patterned surface charge and topography*. Acc Chem Res, 2003. **36**(8): p. 597-604.

Shubin, V.E. and P. Kékicheff, (1993), Electrical Double Layer Structure Revisited via a Surface Force Apparatus: Mica Interfaces in Lithium Nitrate Solutions, p. 108-123.

Chapel, J.P., (1994), Electrolyte Species Dependent Hydration Forces between Silica Surfaces, p. 4237-4243.

Borghi, F., et al., (2013), Nanoscale roughness and morphology affect the IsoElectric Point of titania surfaces, p. e68655.

Duval, J.F., F.A. Leermakers, and H.P. van Leeuwen, (2004), Electrostatic interactions between double layers: influence of surface roughness, regulation, and chemical heterogeneities, p. 5052-65.

Nosrati, R., et al., (2012), Numerical Modeling of Electroosmotic Nanoflows with Overlapped Electric Double Layer, p. 2228-2239.

Huang, K.-D. and R.-J. Yang, (2007), Electrokinetic behaviour of overlapped electric double layers in nanofluidic channels, p.234-256.

Gunsolus, I.L. and C.L. Haynes, (2016), Analytical Aspects of Nanotoxicology, p. 451-79.

Loni, A., et al., (2015), Supercritically-Dried Porous Silicon Powders with Surface Areas Exceeding 1000 m^2/g. p. P289-P292.

Wu, D.X., et al., (2009), Critical Issues in Nanofluids Preparation, Characterization and Thermal Conductivity, p. 103-112.

Yang, Y., et al., (2006), Thermal and rheological properties of carbon nanotube-in-oil dispersions, p.11.

Ojea-Jimenez, I., et al., (2016), Highly Flexible Platform for Tuning Surface Properties of Silica Nanoparticles and Monitoring Their Biological Interaction, p. 4838-4850.

Zane, A., et al., (2015), Uptake of bright fluorophore core-silica shell nanoparticles by biological systems, p. 1547-67.

Maguire, C.M., et al., (2018), Characterisation of particles in solution - a perspective on light scattering and comparative technologies, p. 732-745.

Kosmulski, M., (2020), The pH dependent surface charging and points of zero charge. p. 102064.

Oh, Y.J., et al., (2009), Effect of wall-molecule interactions on electrokinetic transport of charged molecules in nanofluidic channels during FET flow control, p. 1601-8.

Zhang, M.K., et al., (2012), DNA Electrokinetic Translocation through a Nanopore: Local Permittivity Environment Effect, p. 4793-4801.

Jing, D. and B. Bhushan, (2015), Electroviscous effect on fluid drag in a microchannel with large zeta potential, p. 2207-16.

Zhuravlev, L.T., (1993), Surface Characterization of Amorphous Silica - a Review of Work from the Former Ussr, p. 71-90.